

Collision dynamics and reactions of fractional vortex molecules in coherently coupled Bose-Einstein condensates

Minoru Eto^{1,2}, Kazuki Ikeno³, Muneto Nitta^{2,4*}

¹*Department of Physics, Yamagata University, Kojirakawa-machi 1-4-12, Yamagata, Yamagata 990-8560, Japan*

²*Research and Education Center for Natural Sciences, Keio University,
Hiyoshi 4-1-1, Yokohama, Kanagawa 223-8521, Japan*

³*Adavito Inc., Hongo-cho 4-26-12, Bunkyo-ku, Tokyo, 113-033, Japan*

⁴*Department of Physics, Keio University, Hiyoshi 4-1-1, Yokohama, Kanagawa 223-8521, Japan*

(Dated: December 20, 2019)

Coherently coupled two-component Bose-Einstein condensates (BEC) exhibit vortex confinement resembling quark confinement in Quantum Chromo Dynamics (QCD). Fractionally quantized vortices winding only in one of two components are attached by solitons, and they cannot stably exist alone. Possible stable states are “hadrons” either of mesonic type, *i.e.*, molecules made of a vortex and anti-vortex in the same component connected by a soliton, or of baryonic type, *i.e.*, molecules made of two vortices winding in two different components connected by a soliton. Mesonic molecules move straight with a constant velocity while baryonic molecules rotate. We numerically simulate collision dynamics of mesonic and baryonic molecules and find that the molecules swap a partner in collisions in general like chemical and nuclear reactions, summarize all collisions as vortex reactions, and describe those by Feynman diagrams. We find a selection rule for final states after collisions of vortex molecules, analogous to that for collisions of hadrons in QCD.

arXiv:1912.09014v1 [cond-mat.quant-gas] 19 Dec 2019

* meto(at)sci.kj.yamagata-u.ac.jp, nitta(at)phys-h.keio.ac.jp

I. INTRODUCTION

Ultracold atomic gases are experimentally controllable systems offering setups to simulate various problems in physics [1–3]. For instance, Bose-Einstein condensates (BECs) of Bose gases are superfluids admitting quantized vortices, *i.e.*, vortices carrying quantized circulations [4] known as global strings in cosmology, and nucleation of vortices and detecting real time dynamics of them were achieved experimentally recently [5]. Among various systems, coherently coupled two-component BECs realized the JILA group [6, 7] are one of interesting systems even for high energy physics; When two components are different hyperfine components of the same atom, one can introduce a Rabi (Josephson) coupling between them. Then, they allow vortex molecules, fractionally quantized vortices confined by solitons (linearly extended objects) [8], which are suggested to share several properties with confinement phenomena of Quantum Chromo Dynamics (QCD), a theory of the strong interaction consisting of quarks and gluons. Such fractional vortex molecules have been extensively studied theoretically [9–17] including sine-Gordon like solitons [18–21]. Moreover such studies have been extended to three or more components [22–27] as well as spinor BECs [28]. As similarities with QCD, dynamics of a single vortex molecule composed of two fractional vortices were studied [14, 16], for which a vortex in the first component and that in the second component are confined by a sine-Gordon soliton. If the two vortices are at the equilibrium distance, the molecule is static. On the other hand, if they are more separated or pushed to a short distance, the molecule rotates clockwise or counterclockwise, respectively. If they are further pulled to be more separated, the soliton connecting them is broken by creating another pair of fractional vortices, and therefore fractional vortices never been liberated (unless the Rabi coupling is turned off). This situation resembles the confinement of quarks in QCD; QCD vacuum is considered to be a dual superconductor [29–31], where chromo electric fluxes are confined to color electric flux tubes due to magnetic monopole condensations. Then, quarks are confined by color electric flux tubes with energy linearly dependent on the distance between them.

In Ref.[16], we have referred fractionally quantized vortices winding in the first and second components as a up-type vortex (or u-vortex for short) and a down-type vortex (or d-vortex), respectively, borrowing the terminology of quarks in QCD. Similarly, we have called an antivortex of the first (second) component \bar{u} - (\bar{d} -) vortex. In the presence of the Rabi coupling, the elementally topological objects are composite defects of u-, d-vortices and the solitons connecting them. There are two possibilities for the soliton to select the vortices in a pair on its two endpoints: either a vortex and an antivortex in the same component such as u and \bar{u} (d and \bar{d}), or vortices in different species such as u and d (\bar{u} and \bar{d}). We have called the former a mesonic vortex molecule and the latter a baryonic vortex molecule in analogy with QCD; Let us regard quantized circulations n_S as the baryon number in QCD, and the winding n_R of the relative phase between the two components as the color charge. Then, u and d vortices carrying fractional baryon number like quarks carry a color charge and therefore cannot exist alone. On the other hand, mesonic molecules $\bar{u}u$ and $\bar{d}d$ not carrying the baryon number like mesons and baryonic molecules ud carrying one baryon number both do not carry a color charge (color singlets) and therefore can exist stably. See Table as a summary of possible states.

	n_1	n_2	n_S (baryon #)	n_R (color charge)	$2n_R$
u	1	0	1/2	1/2	1
d	0	1	1/2	-1/2	-1
\bar{u}	-1	0	-1/2	-1/2	-1
\bar{d}	0	-1	-1/2	1/2	1
$\bar{u}u$	0	0	0	0	0
$\bar{d}d$	0	0	0	0	0
$\bar{u}d$	-1	1	0	-1	-2
$\bar{d}u$	1	-1	0	1	2
ud	1	1	1	0	0
$\bar{u}\bar{d}$	-1	-1	-1	0	0

TABLE I. Topological winding numbers n_1 , n_2 , n_S and n_R are shown.

In this paper, in order to pursue further similarities between BECs and QCD, we focus on a few body dynamics of vortex molecules, more precisely their collisions, in contrast to previous works focussing on dynamics of either single molecules [14–16] or many molecules describing vortex lattices [12] or Berezinskii-Kosterlitz-Thouless transition [17]. Our numerical studies are twofolds: the meson-meson scattering and the meson-baryon scattering. First, we investigate the meson-meson scattering of the same species ($\bar{u}u$ - $\bar{u}u$). Firstly, we simulate the head-on collisions (zero impact parameter) by varying the incident angles. We show that the constituent vortices swap the partners in collisions. The recombination can be understood as a collision of the SG and anti-SG solitons, and the swapping is

nothing but the pair annihilation and creation of the confining SG solitons. The simulation with the initial relative angle π happens to show the right angle scattering of the two mesons, which is very common among relativistic topological solitons. We then develop a useful description by using the Feynman diagrams. We also study the meson-meson scatterings with non-zero impact parameters.

We then study the meson-meson scattering of the different spices ($\bar{u}u$ - $\bar{d}d$). We find that in head-on collision with the 0 relative angle, the scattering of the two SG solitons occurs. For the head-on collisions with the smaller relative angles, the incoming u and d mesons are converted to the intermediate baryon and anti-baryon pair during the collision. The intermediate baryons rotate, and then they are reformed back into the mesons at the second recombination. Forming the intermediate baryonic state results in the shift of the outgoing line from the ingoing one. We also study the scatterings with non-zero impact parameters in this case too.

Next we study the meson-baryon scatterings ($\bar{u}u$ and ud) and find that the meson and baryon swap their constituent u vortices, and the new meson goes out while the new baryon stays at slightly shifted point from the original baryon point. For scattering of a longer meson to the baryon, the recombination takes place also in this case, so that a longer and kink bend baryon is formed at first stage, and subsequently a long and bent molecule is unstable and soon disintegrates into a set of shorter meson and baryon. As a result, the final state includes more molecules than the initial configuration, resembling what happens in real Hadron collider experiments. We exaggeratedly call it a vortical hadron jet in the VHC (vortical hadron collider) experiment.

We then further discuss a connection between BEC and QCD comparing the Polyakov's dual photon model in $2+1$ dimensions to the low energy effective theory based on two-component BECs. We also point out that the so-called Okubo-Zweig-Iizuka (OZI) rule [32–34] rule in QCD, which is a phenomenological rule concerning with the final state of the collision found in 1960s [35], seems to hold in vortex molecule collisions in BECs.

This paper is organized as follows. In Sec. II, we introduce our model and describe mesonic and baryonic vortex molecules. In Secs. III and IV, we study the meson-meson scattering of the same spices ($\bar{u}u$ - $\bar{u}u$) and of the different spices ($\bar{u}u$ - $\bar{d}d$), respectively. In Sec. V, we study the meson-baryon scatterings ($\bar{u}u$ and ud). In Sec. VI, we give comments on a connection between BEC and QCD. Sec. VII is devoted to a summary and discussion.

II. HADRONIC VORTEX MOLECULES

Theoretically, dynamics of the condensates Ψ_i can be described by the coupled Gross-Pitaevskii (GP) equations

$$\left[i\hbar \frac{\partial}{\partial t} + \frac{\hbar^2}{2m} \nabla^2 - (g_i |\Psi_i|^2 + g_{12} |\Psi_j|^2 - \mu_i) \right] \Psi_i = -\hbar\omega \Psi_i, \quad (i = 1, 2), \quad (1)$$

where $\hat{1} = 2$, $\hat{2} = 1$, g_{ij} represents the atom-atom coupling constants, m is the mass of atom, and μ_i represents the chemical potential. The first and second condensates $\Psi_{1,2}$ are coherently coupled through the Rabi (Josephson) terms with the Rabi frequency ω . Experimentally, such a coherent coupling was achieved by the JILA group [7]. In the following, we assume

$$g_1 = g_2 \equiv g, \quad \mu_1 = \mu_2 \equiv \mu, \quad (2)$$

for simplicity, and focus on a miscible BEC ($g > g_{12}$) in which both condensates coexist with

$$|\Psi_1| = |\Psi_2| = \sqrt{\frac{\mu + \hbar\omega}{g + g_{12}}} \equiv v. \quad (3)$$

If the Rabi interaction is turned off $\omega = 0$, the system has two $U(1)$ symmetries $U(1)_1 \times U(1)_2$ defined by

$$U(1)_1 : (\Psi_1, \Psi_2) \rightarrow (e^{i\alpha_1} \Psi_1, \Psi_2), \quad U(1)_2 : (\Psi_1, \Psi_2) \rightarrow (\Psi_1, e^{i\alpha_2} \Psi_2). \quad (4)$$

These symmetries can also be expressed as

$$[U(1)_S \times U(1)_R] / \mathbb{Z}_2 : (\Psi_1, \Psi_2) \rightarrow (e^{i\alpha} \Psi_1, e^{\pm i\alpha} \Psi_2), \quad (5)$$

where $+$ is for $U(1)_S$ and $-$ is for $U(1)_R$, and \mathbb{Z}_2 represents simultaneous rotations of $U(1)_S$ and $U(1)_R$ with angles $\alpha = \pi$ for both of them, which has been introduced to remove a redundancy. When $\omega \neq 0$, the relative $U(1)_R$ is manifestly broken. Namely, the number of each atom is not preserved but the total number of the first and second atoms is preserved.

In the following, we will numerically solve the GP equation (1). For that purpose it is convenient first to rewrite it in terms of dimensionless variables

$$\tilde{t} = \frac{\mu}{\hbar} t, \quad \tilde{x}_i = \frac{\hbar}{\sqrt{m\mu}} x_i, \quad \tilde{\omega} = \frac{\hbar}{\mu} \omega, \quad \tilde{g}_{12} = \frac{g_{12}}{g}, \quad \tilde{\Psi}_i = \sqrt{\frac{g}{\mu}} \Psi_i. \quad (6)$$

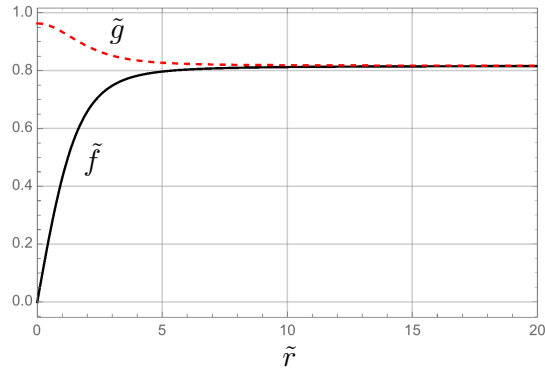


FIG. 1. The profile functions \tilde{f} and \tilde{g} of a u- or d-vortex for $\tilde{g}_{12} = 0.5$. The Rabi term is suppressed ($\tilde{\omega} = 0$).

Then, the GP equation can be rewritten as

$$\left[i \frac{\partial}{\partial t} + \frac{1}{2} \tilde{\nabla}^2 - \left(|\tilde{\Psi}_i|^2 + \tilde{g}_{12} |\tilde{\Psi}_i|^2 - 1 \right) \right] \tilde{\Psi}_i = -\tilde{\omega} \tilde{\Psi}_i, \quad (i = 1, 2). \quad (7)$$

Thus, the essential parameters are only $\tilde{\omega}$ and \tilde{g}_{12} . In what follows, we will assume $\tilde{g}_{12} \neq 1$.

When $\tilde{\omega} = 0$, both the $U(1)_1 \times U(1)_2$ are spontaneously broken in the ground state. As a consequence, there are two kinds of topologically stable vortices supported by topological winding number $\pi_1(U(1)_1 \times U(1)_2) = \mathbb{Z} \times \mathbb{Z}$. A vortex associated with the first $U(1)_1$ at the origin, which we will call the u-vortex, is given by

$$\text{u-vortex: } \tilde{\Psi}_1 = \tilde{f}(\tilde{r}) e^{i\theta}, \quad \tilde{\Psi}_2 = \tilde{g}(\tilde{r}), \quad (8)$$

with $\tilde{r} = \sqrt{\tilde{x}_1^2 + \tilde{x}_2^2}$. Similarly, a vortex associated with the second $U(1)_2$ at the origin, which we will call the d-vortex, is given by

$$\text{d-vortex: } \tilde{\Psi}_1 = \tilde{g}(\tilde{r}), \quad \tilde{\Psi}_2 = \tilde{f}(\tilde{r}) e^{i\theta}. \quad (9)$$

A u-vortex becomes an anti u-vortex (we will refer it to a $\bar{\text{u}}$ -vortex) by exchanging $\theta \rightarrow -\theta$. Similarly, a d-vortex and a $\bar{\text{d}}$ -vortex are replaced by $\theta \rightarrow -\theta$. The profile functions \tilde{f} and \tilde{g} satisfy the following second order ordinary differential equations

$$\left[\frac{1}{2} \left(\frac{\partial^2}{\partial \tilde{r}^2} + \frac{1}{\tilde{r}} \frac{\partial}{\partial \tilde{r}} - \frac{1}{\tilde{r}^2} \right) - \left(\tilde{f}^2 + \tilde{g}_{12} \tilde{g}^2 - 1 \right) \right] \tilde{f} = 0, \quad (10)$$

$$\left[\frac{1}{2} \left(\frac{\partial^2}{\partial \tilde{r}^2} + \frac{1}{\tilde{r}} \frac{\partial}{\partial \tilde{r}} \right) - \left(\tilde{g}^2 + \tilde{g}_{12} \tilde{f}^2 - 1 \right) \right] \tilde{g} = 0. \quad (11)$$

The appropriate boundary conditions are

$$\lim_{\tilde{r} \rightarrow 0} \tilde{f} = 0, \quad \lim_{\tilde{r} \rightarrow \infty} \tilde{f} = \tilde{v}, \quad \lim_{\tilde{r} \rightarrow 0} \frac{\partial \tilde{g}}{\partial \tilde{r}} = 0, \quad \lim_{\tilde{r} \rightarrow \infty} \tilde{g} = \tilde{v}_0, \quad (12)$$

where we have defined

$$\tilde{v}_0 = \frac{1}{\sqrt{1 + \tilde{g}_{12}}}. \quad (13)$$

Fig. 1 shows a typical numerical solution of \tilde{f} and \tilde{g} for $\tilde{g}_{12} = 0.5$ as an example.

It is useful to introduce the pseudo-spin to distinguish u- and d-vortices;

$$\mathbf{S} = -\frac{\tilde{\Psi}^\dagger \boldsymbol{\sigma} \tilde{\Psi}}{\tilde{\Psi}^\dagger \tilde{\Psi}}, \quad \tilde{\Psi} = (\Psi_1, \Psi_2) \quad (14)$$

with the Pauli matrices $\boldsymbol{\sigma}$. \mathbf{S} is a real three-vector satisfying $|\mathbf{S}| = 1$, and so it can be thought of as coordinates of an internal S^2 target space. The pseudo spin \mathbf{S} is transformed as a triplet $\mathbf{3}$ under the $SU(2)$ transformation $\tilde{\Psi} \rightarrow U \tilde{\Psi}$ with $U \in SU(2)$. Note that the $SU(2)$ is only manifest symmetry of a part of the GP equations, namely

the gradient terms of Eq. (1). The rest terms of Eq. (1) generally do not respect the $SU(2)$ symmetry but the subgroup $U(1)_R \subset SU(2)$. Only when $g = g_{12}$ ($\tilde{g}_{12} = 1$) together with the condition (2) holds, the system symmetry $U(1)_1 \times U(1)_2$ is enhanced to $[U(1)_S \times SU(2)]/\mathbb{Z}_2$. Otherwise the $SU(2)$ is only approximate symmetry of generic GP equation (1). The u- and d-vortices have $(\tilde{\Psi}_1(0,0), \tilde{\Psi}_2(0,0)) = (0, \tilde{g}(0))$ and $(\tilde{g}(0), 0)$ at their cores, so that their the pseudo spins are $\mathbf{S} = (0, 0, 1)$ (up) and $\mathbf{S} = (0, 0, -1)$ (down), respectively. Fig. 2 shows the pseudo spins of the u- and d-vortices.

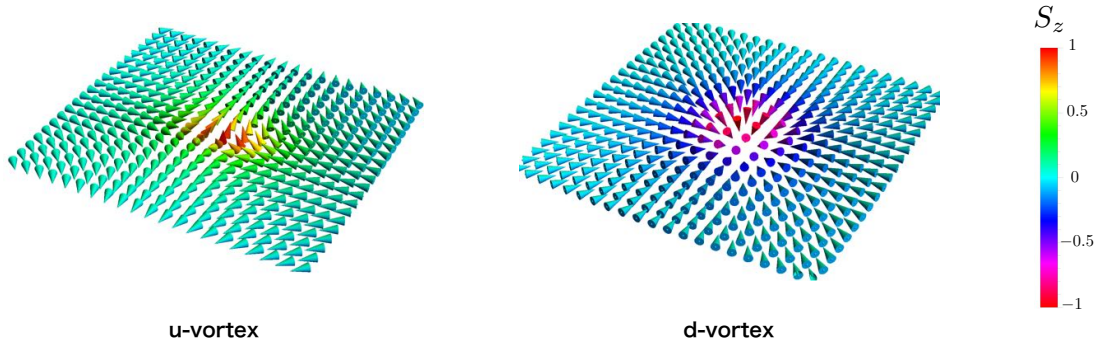


FIG. 2. Vector plots of the pseudo spin $\mathbf{S}(x^1, x^2)$ for the u- and d-vortices (constructed from the solution given in Fig. 1) are plotted on the x^1 - x^2 plane ($\tilde{x}^{1,2} \in [-5, 5]$). The colors of arrows represent S_z . The Rabi frequency is set to be $\tilde{\omega} = 0$.

When $\tilde{\omega} = 0$, the vortex number can be measured by

$$n_i = \frac{1}{2\pi} \oint_C d\theta_i = \frac{1}{2\pi} \int_0^{2\pi} \frac{d\theta_i}{d\theta} d\theta, \quad (15)$$

where θ_i is the phase of Ψ_i ($\theta_i = \arg \Psi_i$), and C is a closed curve in the x^1 - x^2 plane.

When $\tilde{\omega} \neq 0$, neither u- nor d-vortex exists alone since $U(1)_R$ is manifestly broken. The winding numbers n_1 and n_2 are no longer good topological numbers. The Rabi term effectively works as a sine-Gordon (SG) type potential

$$V_{\text{Rabi}} = -2\hbar\omega v^2 \cos(\theta_1 - \theta_2), \quad (16)$$

where we have set $\psi_i = v e^{i\theta_i}$. Due to this, the u-vortex given in Eq. (8) with $(\theta_1, \theta_2) = (\theta, 0)$ is inevitably attached by a SG soliton at $\theta = \pi$. By the same reason, the d-vortex given in Eq. (9), \bar{u} -vortex and \bar{d} -vortex are also attached by a SG or an anti SG soliton. Under the nonzero $\tilde{\omega}$, it turns out that the followings are more useful than n_1 and n_2

$$n_S = \frac{1}{2\pi} \oint_C d\theta_S = \frac{1}{2\pi} \int_0^{2\pi} \frac{1}{2} \left(\frac{d\theta_1}{d\theta} + \frac{d\theta_2}{d\theta} \right) d\theta = \frac{n_1 + n_2}{2}, \quad (17)$$

$$n_R = \frac{1}{2\pi} \oint_C d\theta_R = \frac{1}{2\pi} \int_0^{2\pi} \frac{1}{2} \left(\frac{d\theta_1}{d\theta} - \frac{d\theta_2}{d\theta} \right) d\theta = \frac{n_1 - n_2}{2}, \quad (18)$$

with $\theta_S = (\theta_1 + \theta_2)/2$ and $\theta_R = (\theta_1 - \theta_2)/2$. Here, n_S and n_R are topological invariants taking values in half integers when $\tilde{\omega} = 0$. Once we turn on $\tilde{\omega} \neq 0$, n_R is no longer a topological number. Though n_R is not preserved, it has another physical meaning: $2n_R$ corresponds to the total SG soliton number across the curve C. For a single u-vortex, we have $2n_R = 1$ for any C which encloses it. We summarize n_1 , n_2 , n_S and n_R in Table I. From this, we see that u- and \bar{d} -vortices are attached by a SG soliton while \bar{u} - and d-vortex are attached by an anti SG soliton.

However, this is only a static picture. Since a semi-infinitely long soliton costs infinite energy, it is dynamically unstable and disintegrate into shorter solitons. A finite soliton is terminated by two vortices, namely it forms a vortex molecule with the SG soliton bounding two vortices. We can figure out all possible types of molecules by seeing n_R . Since a vortex molecule is finite configuration, the corresponding n_R for a sufficiently large C enclosing it must be zero. Therefore, there exist four kinds of molecules, $\bar{u}\bar{u}$, $\bar{d}\bar{d}$, $u\bar{d}$, and $\bar{u}d$. We plot the pseudo spins of $\bar{u}\bar{u}$ and $u\bar{d}$ molecules in Fig. 3.

This phenomenon resembles quark confinement in QCD. The quarks are elementary particles in nature, but they are confined in the form of hadrons and we cannot take any quarks out from hadrons. Quarks in QCD resemble our ‘‘elementary’’ u- and d-vortices in the 2 component BECs. One might envisage that the isospin of up and down quarks is a natural counterpart of the pseudo spin. Furthermore, as is well known, a hadron consists of several quarks whose

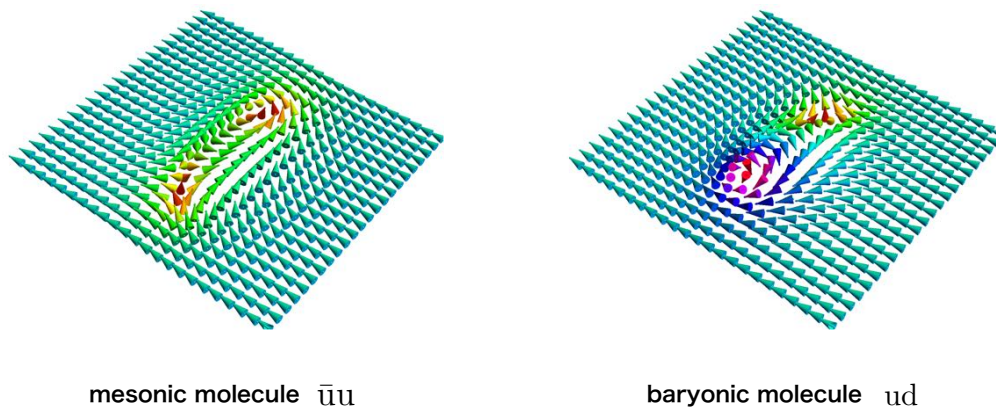


FIG. 3. Vector plots of the pseudo spin $\mathbf{S}(x^1, x^2)$ for the $\bar{u}u$ and ud are plotted on the x^1 - x^2 plane. The plot region of the left panel is $\tilde{x}^1 \in [-10, 10]$ and $\tilde{x}^2 \in [40, 60]$, and that for the right panel is $\tilde{x}^1 \in [-10, 10]$ and $\tilde{x}^2 \in [-10, 10]$. The color map is the same as the one in Fig. 2. The Rabi frequency is set to be $\tilde{\omega} = 0.05$.

total color charge is zero (singlet of $SU(3)$ color group). Now, it is natural to relate the $U(1)_R$ winding number n_R of the “elementary” vortices (u, d, \bar{u}, \bar{d}) with the color charge of the quarks. Namely, a hadron in the two component BECs is singlet by means of $n_R = 0$. Moreover, we can also relate the $U(1)_S$ winding number n_S of the elementary vortices (u - and d -vortices have $1/2$, and \bar{u} - and \bar{d} - have $-1/2$ winding number) with the baryon number of the quarks (a quark has $1/3$ and an anti quark has $-1/3$ baryon number). A hadron with the baryon number $+1(-1)$ are called a baryon (an anti-baryon), and that with no baryon number is called a meson in QCD. Borrowing the terminology from QCD, we may refer a ud vortex molecule to a baryon since it has $n_S = 1$, and the $\bar{u}\bar{d}$ vortex molecule to an anti-baryon with $n_S = -1$. Similarly, we call the $\bar{u}u$ molecule as a u meson while the $\bar{d}d$ molecule as a d meson because they have $n_S = 0$. Of course, though this analogy between the two component BECs and QCD is limited, it is very useful. For example, there does not exist $\bar{u}d$ meson in the BEC system because its $U(1)_R$ winding number is not zero, see Table I. We will give more discussions on a relation between QCD and BECs in Sec. VI.

Let us next mention the dynamics of the mesonic and baryonic vortex molecules. A meson goes straight with an almost constant velocity toward the direction perpendicular to the molecule. This motion can be understood by a Magnus force between the vortex and anti-vortex in the meson. For a longer meson the attractive force is dominated by the SG soliton and therefore the moving speed is almost constant. On the other hand, the attractive force originated by the inter-vortex force dominates for a shorter meson. Therefore, the shorter meson moves faster. However, these observations are valid only for a meson with reasonable length. If the meson is too short, it soon decays. If the meson is too long, it soon disintegrates [16]. We show a typical motion of a u meson in Fig. 4. We put a meson whose length is about 10 in terms of the dimensionless coordinate \tilde{x}_i . We put the meson at $(\tilde{x}_1, \tilde{x}_2) = (0, 50)$ at $\tilde{t} = 0$ (the pseudo spin of the initial state is given in the left panel of Fig. 3). It moves down and passes the origin around $\tilde{t} = 100$. During the run, the soliton periodically bends forward and backward, and distance between u and \bar{u} periodically gets shorter and longer.

On the other hand, a baryon moves very differently. It does not run but rotates with an almost constant angular speed [14, 16]. When the baryon is longer, the motion is dominated by attractive force due to the soliton. On the other hand, when the baryon is shorter, the soliton tension and the inter-vortex force compete. When $g_{12} > 0$, the inter-vortex force is repulsive [36]. The shorter the baryon is, the stronger the inter-vortex force is. On the contrary, when the baryon is too short, the soliton tension becomes negligible. Therefore, the rotating speed of the baryon for $g_{12} > 0$ becomes gradually smaller and it vanishes at an equilibrium. For the baryon with $g_{12} < 0$, both the inter-vortex interaction and soliton tension give attractive forces [36] so that there does not exist such an equilibrium. Similarly to the meson, too long baryon soon disintegrates. However, the baryon never vanishes since the $U(1)_S$ winding number is topological. Fig. 4 shows a typical rotating baryon. We put the baryon of the length about 8 in the dimensionless unit at the origin at $\tilde{t} = 0$ (the pseudo spin of the initial state is given in the right panel of Fig. 3). It rotates clockwise and return to the original angle around $\tilde{t} = 90$. As meson, it slightly vibrates during the rotation. Baryons shorter than equilibrium distance rotate counterclockwise.

Before closing this section, let us mention significant difference between relativistic and non-relativistic dynamics of vortices. Both straight moving of the mesonic molecule and rotation of the baryonic molecule are peculiar to non-relativistic system. Due to these characteristic motions, molecules are quasi stable. On the contrary, in relativistic systems two vortices separate (close on) when the inter vortex force is repulsive (attractive), so that no stable

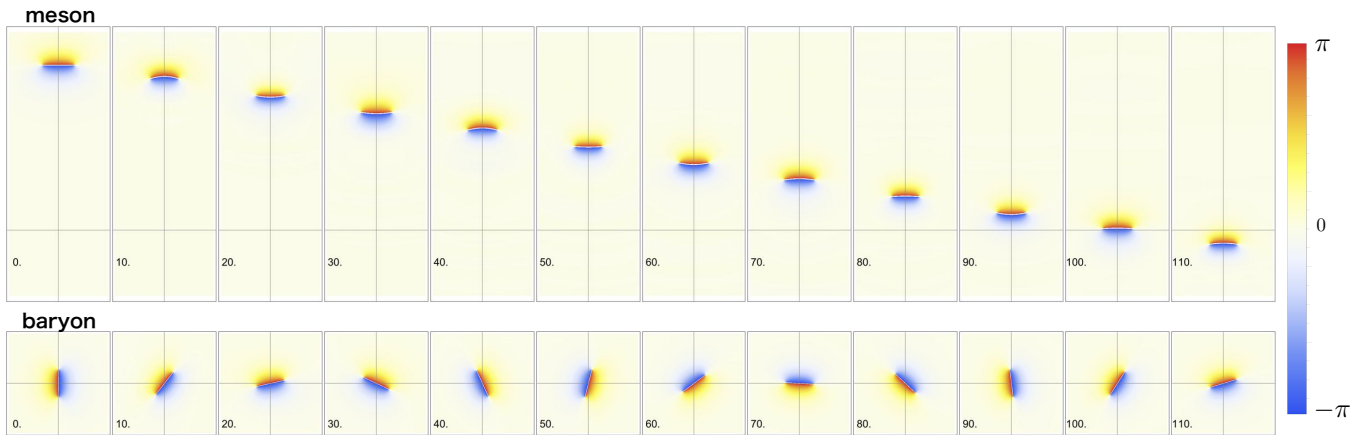


FIG. 4. The upper panel shows a motion of a u meson, and the lower panel shows a motion of a baryon. We choose $\tilde{g}_{12} = 0.5$ and $\tilde{\omega} = 0.05$. The color corresponds to $\arg(\Psi_1) - \arg(\Psi_2)$. The red corresponds to $\arg(\Psi_1) - \arg(\Psi_2) = \pi$ while the blue corresponds to $\arg(\Psi_1) - \arg(\Psi_2) = -\pi$. The upper panel ($\tilde{x}_1 \in [-15, 15]$, $\tilde{x}_2 \in [-20, 60]$): We put \bar{u} -vortex at $(\tilde{x}_1, \tilde{x}_2) = (-5, 50)$ and u-vortex at $(\tilde{x}_1, \tilde{x}_2) = (5, 50)$ at $\tilde{t} = 0$ in the left-most figure. The lower panel ($\tilde{x}_1 \in [-15, 15]$, $\tilde{x}_2 \in [-15, 15]$): we put u-vortex at $(\tilde{x}_1, \tilde{x}_2) = (0, 4)$ and d-vortex at $(\tilde{x}_1, \tilde{x}_2) = (0, -4)$ at $\tilde{t} = 0$. To see motions of the molecules, we also show snapshots with interval $\delta\tilde{t} = 10$.

molecules in general exist. In what follows, we will make use of these non-relativistic property, and numerically simulate scatterings of mesonic and baryonic molecules in two-component BECs as a vortical hadron collider.¹

Here, one comment is in order. Vortex dynamics in two-component BEC in the absence of the Rabi interaction was studied in Ref. [37, 38] in which case fractional vortices are liberated. Even in such a case, dynamics is quite nontrivial but it is out of the scope of the present paper.

III. MESON-MESON SCATTERING: THE CASE OF $\bar{u}u$ - $\bar{u}u$

A. $\bar{u}u$ - $\bar{u}u$ head-on collision

Let us begin with the most elementary process, namely head-on collision of two mesons of the same species. Since we have concentrated on the symmetric model under replacement Ψ_1 and Ψ_2 , we can choose the u mesons without loss of generality. We prepare an initial configuration as follows. First, we create a configuration $(\Psi_1^{(1)}, \Psi_2^{(1)})$ for the u meson ($\bar{u}_1 u_1$) corresponding to the one given in the left-most panel of the first row in Fig. 4. Similarly, we prepare another configuration $(\Psi_1^{(2)}, \Psi_2^{(2)})$ for the u meson ($\bar{u}_2 u_2$) by rotating the $\bar{u}_1 u_1$ by 180 degree around the origin. Then, we superpose these two configurations à la the Abrikosov as

$$\Psi_i^{(\text{ini})} = \frac{1}{v} \Psi_i^{(1)} \Psi_i^{(2)}, \quad (i = 1, 2). \quad (19)$$

In this way, we have the initial configuration which has two incoming mesons $\bar{u}_1 u_1$ at $(\tilde{x}_1, \tilde{x}_2) = (0, 50)$ [precisely speaking, we put a u vortex at $(\tilde{x}_1, \tilde{x}_2) = (5, 50)$ and a \bar{u} vortex at $(\tilde{x}_1, \tilde{x}_2) = (-5, 50)$] and the $\bar{u}_2 u_2$ and $(\tilde{x}_1, \tilde{x}_2) = (0, -50)$ [we put a u vortex at $(\tilde{x}_1, \tilde{x}_2) = (-5, -50)$ and a \bar{u} vortex at $(\tilde{x}_1, \tilde{x}_2) = (5, -50)$]. With the initial configuration at hand, next we numerically integrate the Gross-Pitaevskii equations. The result is shown in Figs. 5 and 6.

Up to slightly before the moment of the collision ($\simeq 100$), each meson goes straight toward the origin as if the other meson does not exist. However, an interesting vortical reaction occurs during the collision. It is a recombination of the SG solitons binding the constituent vortices \bar{u} and u. Before the collision $\bar{u}_1 u_1$ and $\bar{u}_2 u_2$ are well separated, and the SG solitons bridge \bar{u}_1 and u_1 , and also \bar{u}_2 and u_2 , respectively. As can be seen in Fig. 6, \bar{u}_1 and u_2 (u_1 and \bar{u}_2) collide head-on, so that two distances between \bar{u}_1 and u_1 , and \bar{u}_1 and u_2 become comparable about the moment of the collision. Then, the SG solitons reconnect different pair of \bar{u} and u from the initial pairs. The new SG solitons

¹ The movies of our numerical simulations studied below are available as the Supplemental Material.

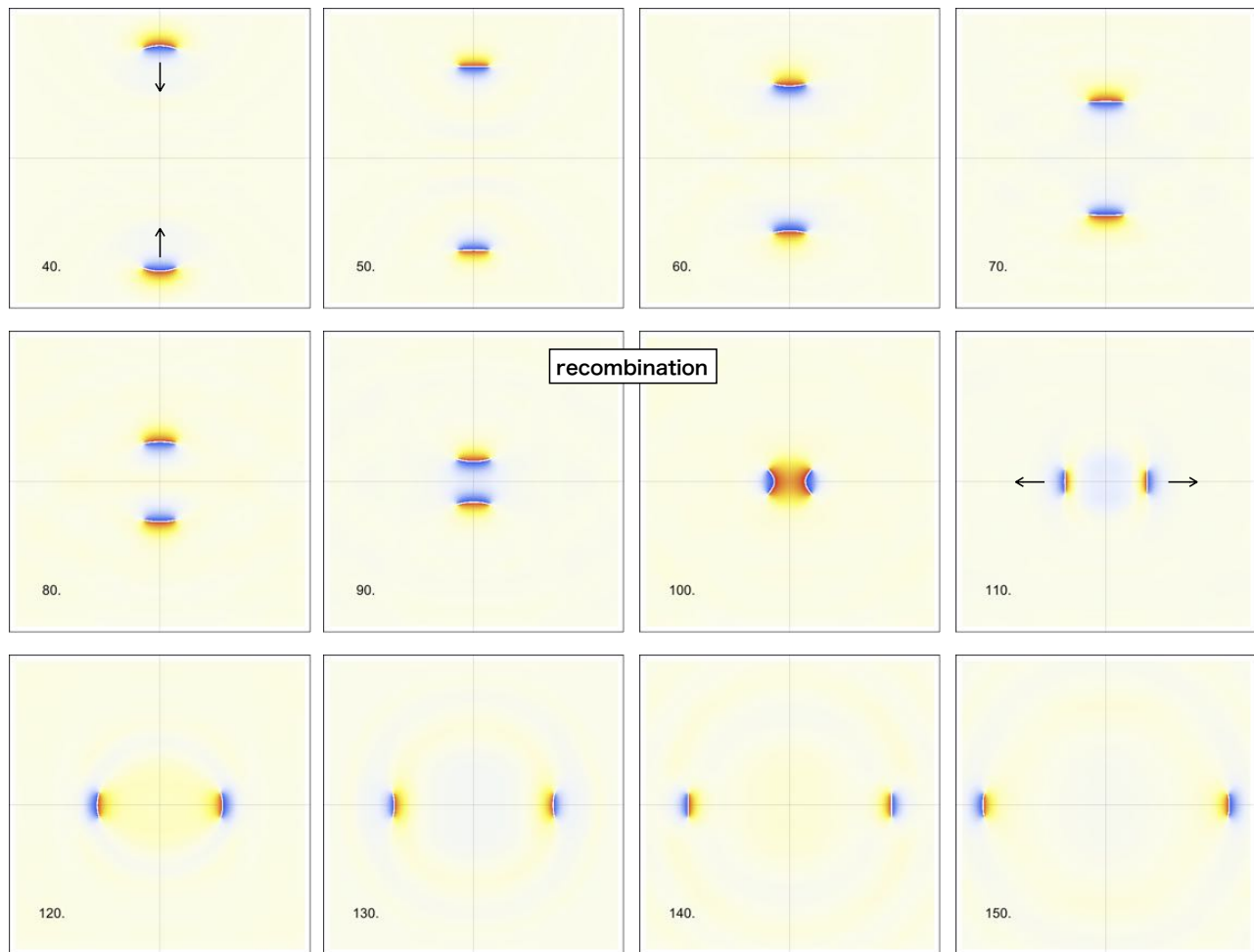


FIG. 5. Two u mesons scattering : Color density plots of the relative phase $\arg(\Psi_1) - \arg(\Psi_2)$. We initially ($\tilde{t} = 0$) set the same u meson ($\bar{u}_1 u_1$) at $(\tilde{x}_1, \tilde{x}_2) = (0, 50)$ as the one given in the left-most panel of the upper line of Fig. 4, and the same u meson ($\bar{u}_2 u_2$) but rotated by 180 degree at $(\tilde{x}_1, \tilde{x}_2) = (0, -50)$. They straightly run with almost constant speed and collide around the origin. During the collision, the sine-Gordon (SG) solitons partially reconnect and the recombination takes place. As a consequence, the u mesons in the head-on collision scatter through a right angle. We show the snapshots from $\tilde{t} = 40$ to 150 with an interval $\delta\tilde{t} = 10$, and the plot region is $\tilde{x}_{1,2} \in [-40, 40]$.

are vertical, so that the new outgoing mesons fly along the x^1 -axis. Namely, the u mesons in the head-on collision scatter through a right angle as a consequence of the recombination. We may describe this process as follows

$$\bar{u}_1 u_1 + \bar{u}_2 u_2 \rightarrow \bar{u}_1 u_2 + \bar{u}_2 u_1. \quad (20)$$

Note that the subscriptions (1 and 2) are introduced just for our convenience; The u_1 and u_2 vortices are the same vortices, so they are indistinguishable. In analogy with chemical and nuclear reactions, we call processes concerning vortex molecules such as Eq. (20) as “vortical reactions.”

Note also that the right angle scattering of two topological solitons are common in relativistic field theories. For instance, magnetic monopoles, vortices and so on do so. However, the right angle scattering is usually observed in the collisions of two solitons with the same topological charges. The right angle scattering here is very different since mesons have zero topological charge and it occurs as a consequence of the recombination.

Let us observe the recombination phenomena more carefully. Fig. 7 shows snapshots in close-up at $\tilde{t} = 95, 97.5, 100, 102.5$. We should pay attention to the orientation of the SG solitons. Looking at the left-most panel at $\tilde{t} = 95$ of Fig. 7 from the top to the bottom along the \tilde{x}^2 -(vertical) axis, the color firstly changes from red to blue representing the upper SG soliton, and then it changes back from blue to red representing the lower SG soliton. The deepest red region corresponds to $\theta_1 - \theta_2 = \pi$ while the deepest bluish region corresponds to $\theta_1 - \theta_2 = -\pi$. Thus, when we focus on the SG solitons, the head-on collision of the two u mesons is nothing but a scattering of the SG and anti-SG solitons. As

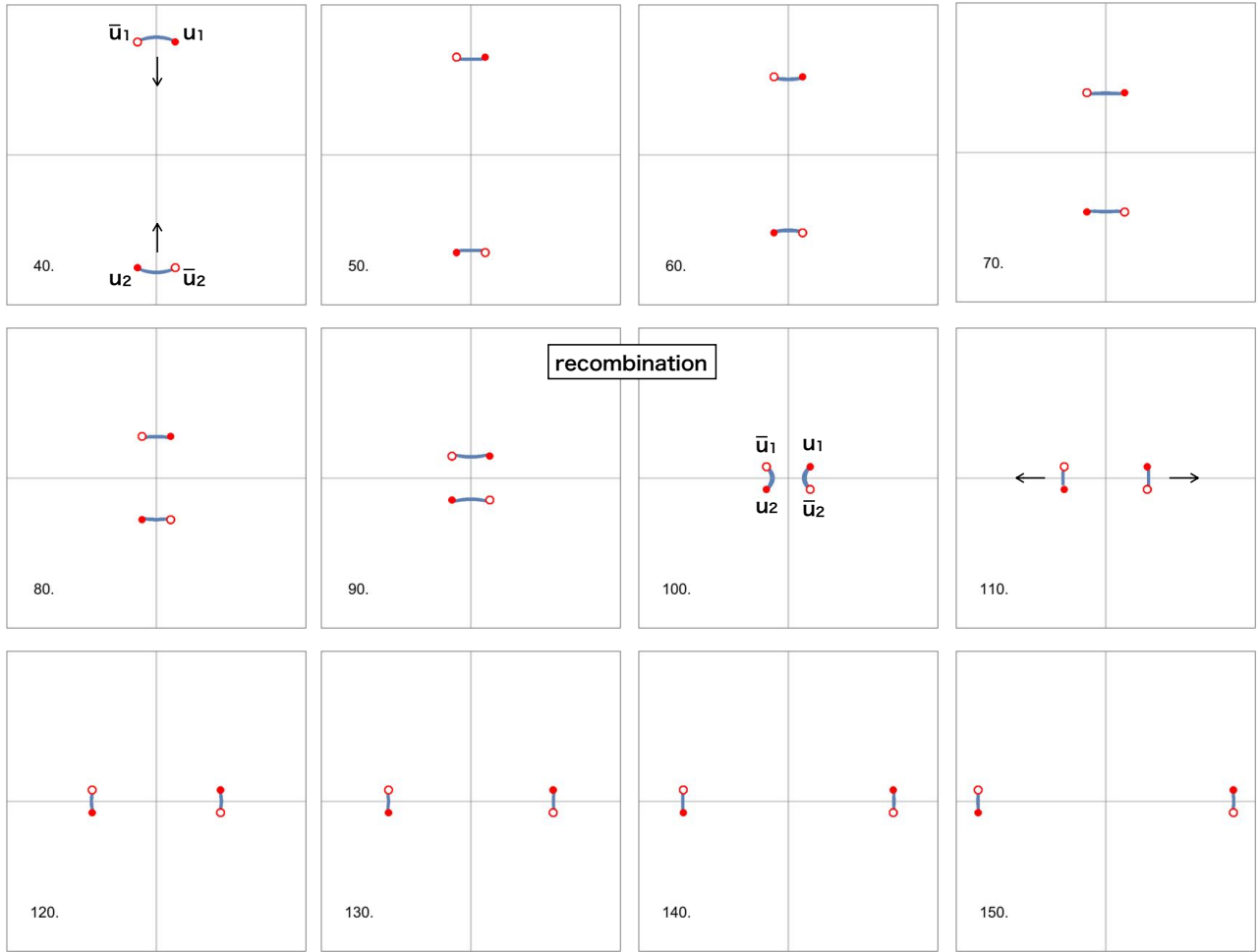


FIG. 6. A simplified plot of the u mesons scattering shown in Fig. 5. We put painted red disks (unpainted red circle) at the points corresponding to the u (\bar{u}) vortex centers. Gray regions bridging the u and \bar{u} vortices show the SG solitons. The gray regions are those where the relative phases take the values within $3 \leq |\arg(\Psi_1) - \arg(\Psi_2)| \leq \pi$, which are numerically obtained from Fig. 5. It is easier to figure out the vortex and anti vortex in this representation than Fig. 5.

can be seen in the panel at $\tilde{t} = 97.5$ of Fig. 7, the SG soliton and anti-SG soliton greatly bend especially around their centers due to an attractive force so that they collide before the u and \bar{u} vortices at the edges of the SG solitons do. Then, their tips annihilate to each other, and they proceed to complete the recombination process, see transformation from $\tilde{t} = 97.5$ to $\tilde{t} = 100$ shown in Fig. 7. The annihilation of the SG soliton and anti solitons can be clearly seen in Fig. 8 where we plot the relative phase $\theta_1 - \theta_2$ on the \tilde{x}^2 -axis by the blue curve. The SG soliton corresponds to the jump $\pi \rightarrow -\pi$ from left to right of the horizontal axis (the \tilde{x}^2 -axis) while the anti-SG soliton corresponds to the opposite jump from $-\pi \rightarrow \pi$. They collide and annihilate about $\tilde{t} = 100 \sim 110$. To be complete, let us also look at the relative phase along the \tilde{x}^1 -axis. It is also plotted in Fig. 8 by the red broken curve. The horizontal axis corresponds to the \tilde{x}^1 -axis for the red broken curves. Before the collision, no SG solitons exist along the \tilde{x}^1 -axis. However, as the SG and anti SG solitons along the \tilde{x}^2 -axis annihilate, a new pair of the SG and anti-SG solitons on the \tilde{x}^1 -axis is created. Hence, we find that the recombination phenomenon is taken over by the pair annihilation and creation of the SG solitons.

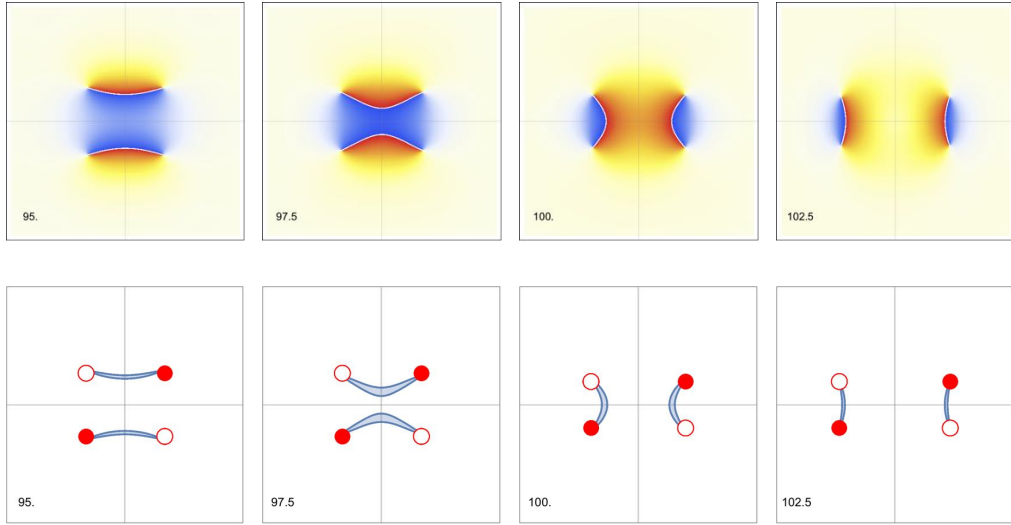


FIG. 7. Snapshots in close-up for $\tilde{x}_i \in [-15, 15]$ at $\tilde{t} = 95, 97.5, 100, 102.5$ for the u meson scattering given in Figs. 5 and 6. The horizontal SG soliton incoming from the top and the anti-soliton from the bottom gradually bend as they are close by, and they partially annihilate at the tips and reconnect to form the vertical SG solitons.

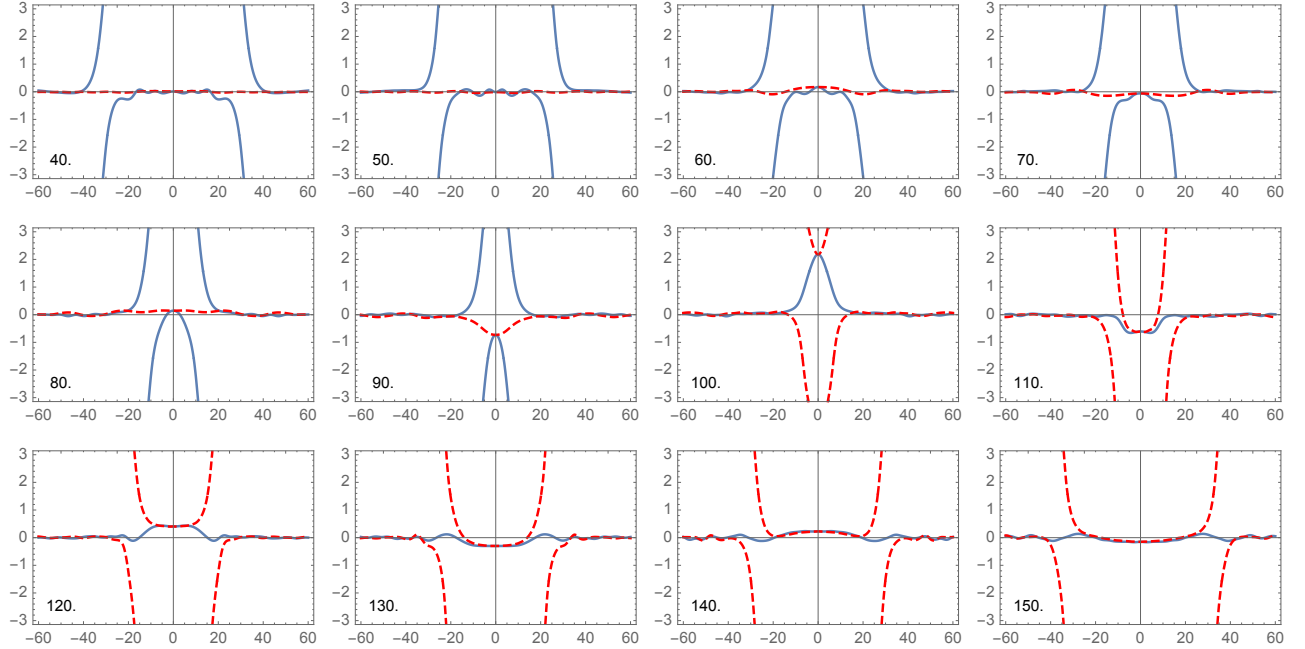


FIG. 8. The phase plots corresponding to the u meson collision in Fig. 5. The solid blue curves show the relative phase $\arg(\Psi_1) - \arg(\Psi_2)$ along the \tilde{x}_2 -axis of Fig. 5. The SG soliton coming from the right-hand side and the anti-SG soliton coming from the left-hand side collide and annihilate. Similarly, the broken red curves show $\arg(\Psi_1) - \arg(\Psi_2)$ along the \tilde{x}_1 -axis of Fig. 5. The SG and anti-SG solitons are pairwise created around the moment of collision.

B. $\bar{u}u$ - $\bar{u}u$ scattering at $\pi/8$ angle

Let us next study u meson scattering similar to that in Sec. III A, but in this time the upper and lower mesons are rotated by $-\pi/8$ and $\pi/8$ from those in Fig. 5. One can see how the scattering is going on in Figs. 9 and 10. Indeed,

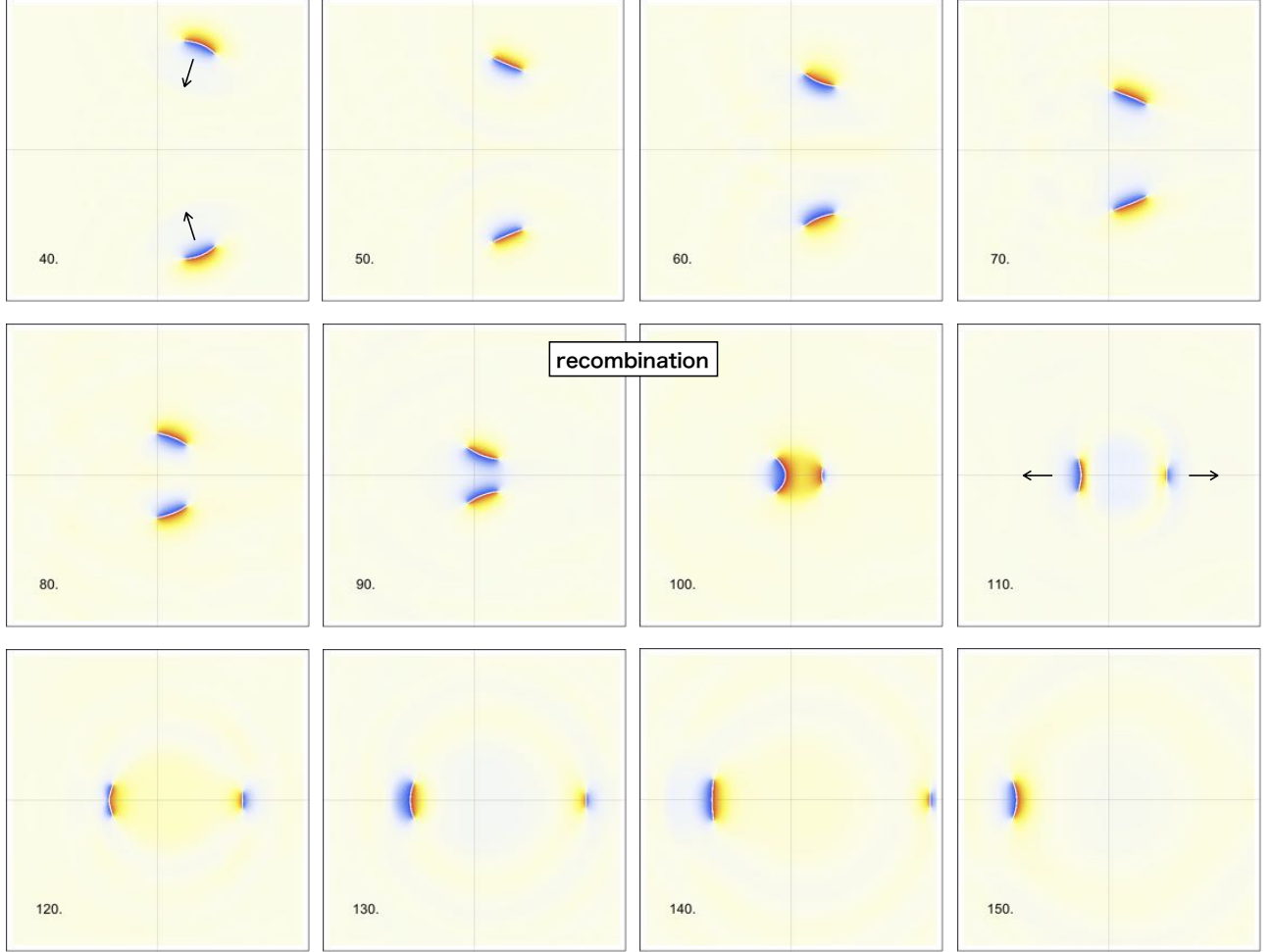


FIG. 9. Two slightly tilted u mesons scattering : Color density plots of the relative phase $\arg(\Psi_1) - \arg(\Psi_2)$. We initially ($\tilde{t} = 0$) set the u meson ($\bar{u}_1 u_1$) at $(\tilde{x}_1, \tilde{x}_2) = (50 \sin \pi/8, 50 \cos \pi/8)$, and the other u meson ($\bar{u}_2 u_2$) at $(\tilde{x}_1, \tilde{x}_2) = (50 \sin \pi/8, -50 \cos \pi/8)$. We only show the snapshots from $\tilde{t} = 40$ to 150 with interval $\delta\tilde{t} = 10$, and the plot region is $\tilde{x}_{1,2} \in [-40, 40]$.

it goes qualitatively in the same way as the previous case. The mesons go straight with almost constant speed until they are close by, then a recombination takes place during the collision. Due to the tilts of incoming mesons, newly formed mesons are in different sizes and scatter off toward the left and right directions as the previous case. The asymmetry can also be seen in the speeds of the out-going mesons. The meson $\bar{u}_1 u_2$ moves faster than the meson $\bar{u}_2 u_1$ as shown in Fig. 10. This is because the former is shorter than the latter. Fig. 11 shows snapshots in close-up at $\tilde{t} = 92.5, 95, 97.5, 100$, in which we again observe that a partial annihilation of the SG and anti-SG solitons leads to the recombination. Compared to the previous case, bend of the SG solitons are milder, because the bending points are not the center and are shifted towards the edges u_1 and \bar{u}_2 .

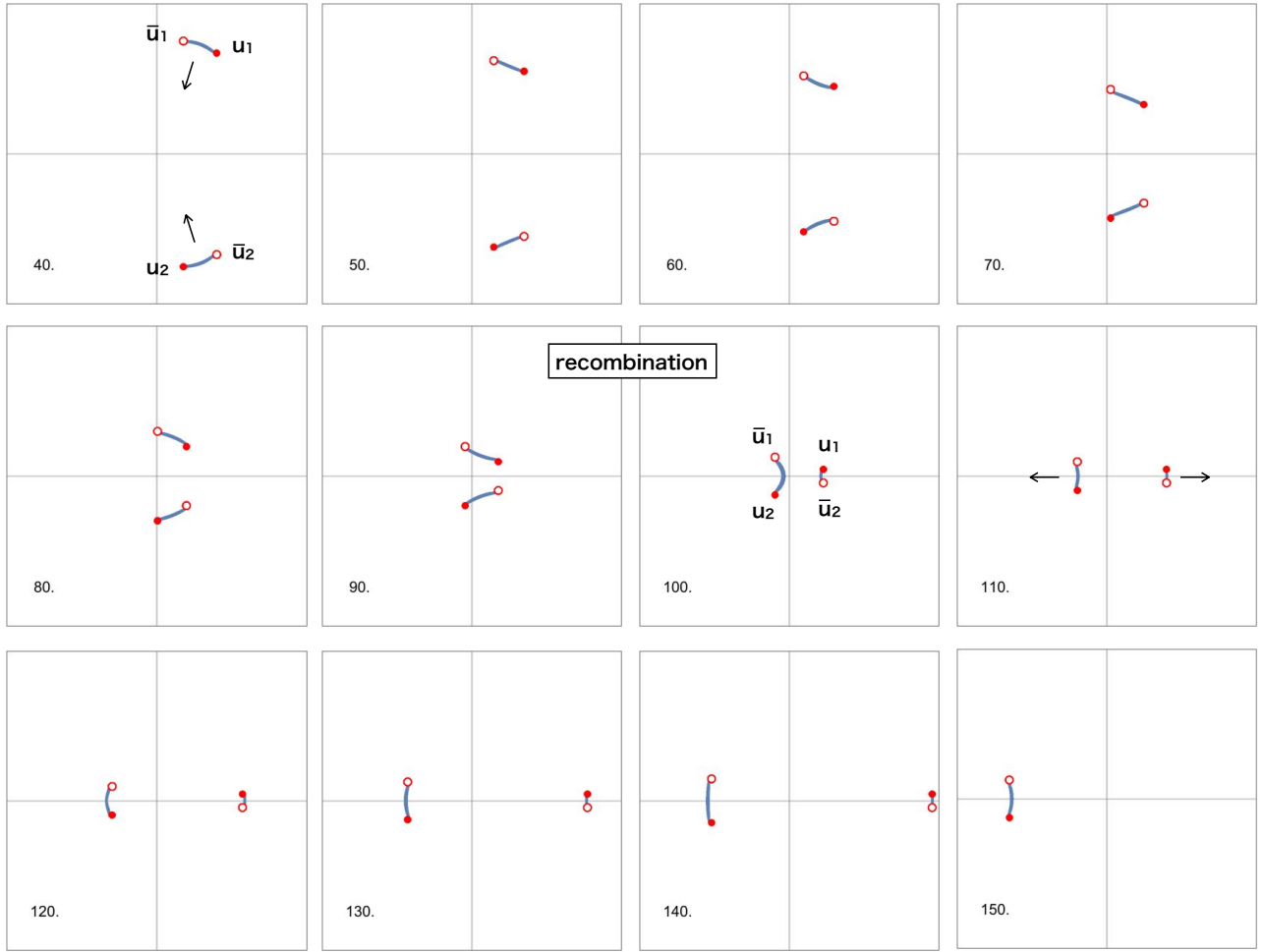


FIG. 10. A simplified plot of the u mesons scattering shown in Fig. 9. For details, see the caption of Fig. 6.

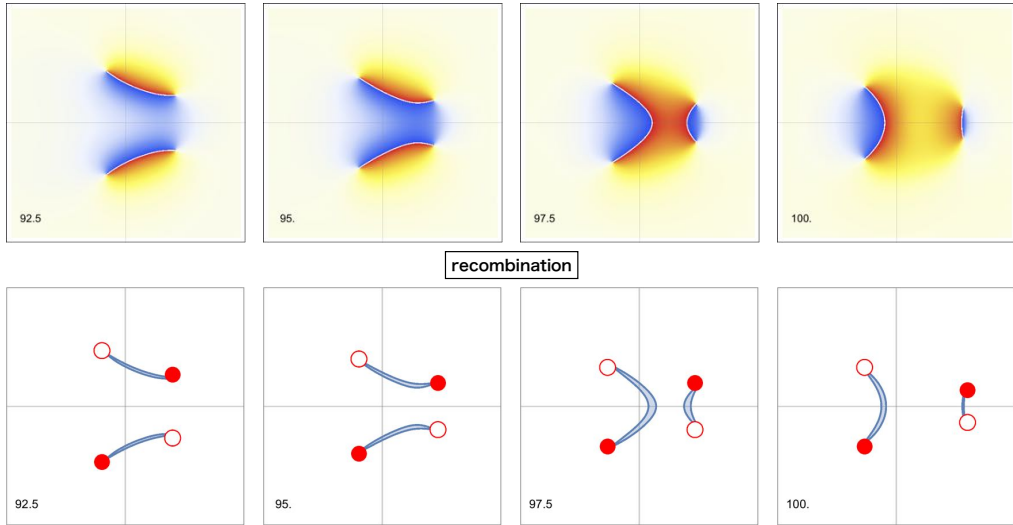


FIG. 11. Snapshots in close-up for $\tilde{x}_i \in [-15, 15]$ at $\tilde{t} = 92.5, 95, 97.5, 100$ for the u meson scattering given in Figs. 9 and 10. The points where the incoming SG solitons steeply bend are not the centers. The incoming SG solitons partially annihilate around the steepest bending point and reconnect to form vertical SG solitons.

C. $\bar{u}u$ - $\bar{u}u$ scattering at $\pi/4$ angle

Let us attempt to simulate one more u meson scattering experiment by rotating further the incoming mesons by $\pi/4$. As expected, the motion of the mesons before the collision is almost unchanged from the previous two cases, see Fig. 12. On the contrary, the states after the collision are distinctive. Firstly, we only observe one meson \bar{u}_1u_2 after the collision. Looking at the moment of the collision in more details, the very short \bar{u}_2u_1 is created but it is soon annihilated, see Fig. 13. This occurs because the relative angle of the incoming mesons is too large. If we further rotate the initial mesons, there is not enough period for the SG solitons to bend to be annihilated. Then, the constituent vortices, u_1 and \bar{u}_2 , are annihilated and the two SG solitons join to form a long \bar{u}_1u_2 meson.

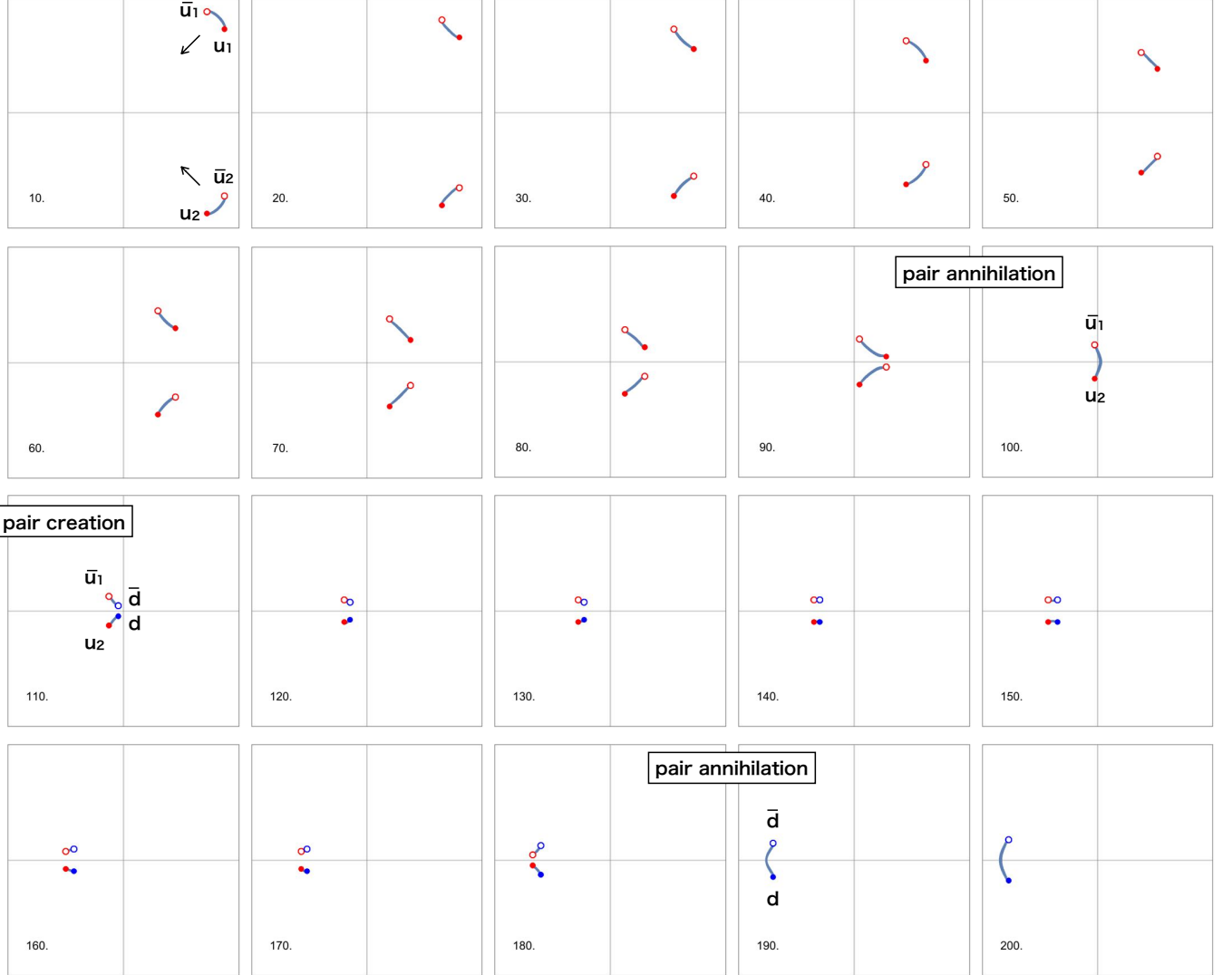


FIG. 12. Two tilted u meson scattering with $\pi/4$ angle: We initially ($\tilde{t} = 0$) set one u meson (\bar{u}_1u_1) at $(\tilde{x}_1, \tilde{x}_2) = (50 \sin \pi/4, 50 \cos \pi/4)$, and the other u meson (\bar{u}_2u_2) at $(\tilde{x}_1, \tilde{x}_2) = (50 \sin \pi/4, -50 \cos \pi/4)$. We only show the snapshots from $\tilde{t} = 10$ to 200 with interval $\delta\tilde{t} = 10$, and the plot region is $\tilde{x}_{1,2} \in [-40, 40]$.

After the collision, the long meson \bar{u}_1u_2 runs toward the left but such a long meson is unstable. As can be seen in Fig. 13, it soon breaks up into two pieces, the baryon (u_2d) and the anti-baryon ($\bar{u}_1\bar{d}$), by creating d and \bar{d} vortices at the center of the long SG soliton. It is notable that this process is peculiar to the 2 component BECs and it never happens in scalar BEC systems. The baryon u_2d spins clockwise whereas the anti-baryon spins counterclockwise, see the panels with $\tilde{t} = 120 \sim 180$ of Fig. 12. At the same time, the pair of baryon and anti-baryon behave as a pair of an integer vortex and an anti-integer vortex. Thus, the baryon and anti-baryon move parallel toward the left direction. After a while, the baryon and anti-baryon join to form a meson $\bar{d}d$ with \bar{u}_1 and u_2 being annihilated.

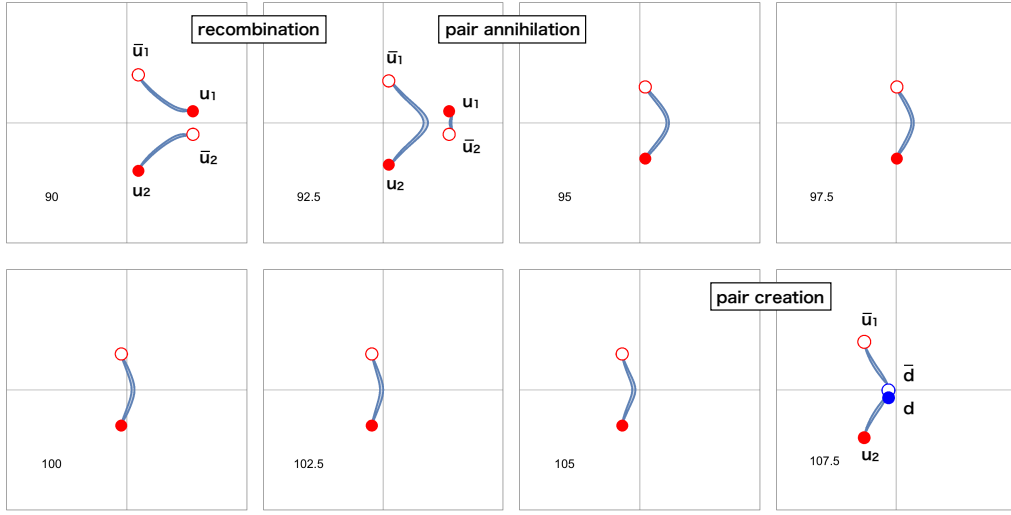
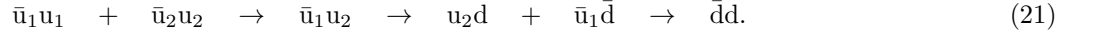


FIG. 13. Snapshots in close-up for $\tilde{x}_i \in [-15, 15]$ at $\tilde{t} = 90, 92.5, 95, 97.5, 100, 102.5, 105, 107.5$ for the u meson scattering given in Figs. 12. The recombination, the pair annihilation of $\bar{u}u$, and the pair creation of $\bar{d}d$ occurs in order.

Thus the corresponding reaction process can be summarized as



Note that the baryon number is preserved to be 0 throughout the reaction.

D. Interaction vertices and Feynman diagrams

Let us summarize the two u meson head-on scattering given above. We found that the scattering sensitively depends on the collision angle which is direct evidence for a meson to have a substructure. We have shown the three examples the head-on collisions with the relative angle π in Fig. 6, $3\pi/4$ in Fig. 10, and $\pi/2$ in Fig. 12. An overview of the scatterings is shown in Fig. 14.

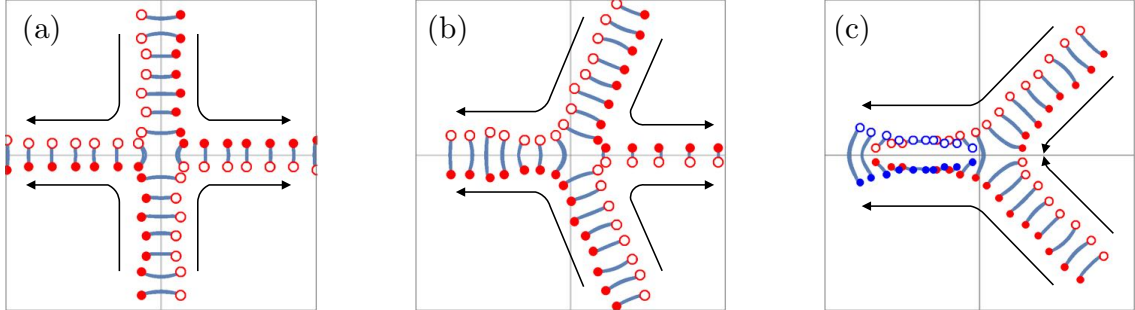


FIG. 14. Summary on u meson and u meson collider experiments: (a) corresponds to Fig. 6, (b) to Fig. 10, and (c) to Fig. 12.

Here, we describe these results by a particle physics point of view. We first deal with the first process given in (a) of Fig. 14 whose vortical reaction is given in Eq. (20). The two incoming u mesons scatter into the two outgoing u mesons. We interpret this process as an elementary interaction among mesons. Namely, this yields a meson-meson-meson-meson vertex. In order to emphasize this view point, let us give a 3D spacetime (2 spatial and 1 temporal) diagram given in the left figure of Fig. 15. It corresponds to the scattering experiment of (a) of Fig. 14, consisting of the world lines of the constituent vortices together with the world sheet of the SG solitons. The 3D diagram can be further simplified as the right figure of Fig. 15. It is a 2D diagram and resembling the so-called twig diagram (a sort

of Feynman diagram which includes only quark lines) known in QCD [33]. Resembling standard Feynman diagrams in quantum field theories, an anti-vortex is represented by a line with an arrow opposite to the time evolution. Thus, we find a four meson vertex as an elemental interaction among mesons.

The second process corresponding (b) of Fig. 14 is essentially same as (a). So the scattering (b) is also described by the same 4 meson vertex in Fig. 15.

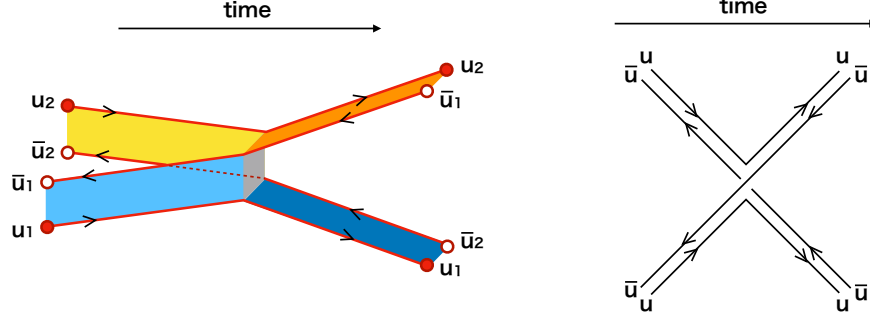


FIG. 15. Meson-meson-meson-meson vertex: The left panel is a 3D diagram describes (a) of Fig. 14. The right panel is a Feynman diagram which is a simplified 2D expression of the left one.

Next, let us make a diagram for the third process (c) of Fig. 14. This scattering is more complicated. Indeed, the corresponding reaction formula given in Eq. (21) consists of three proceeding steps. The Feynman diagram for this scattering is given in Fig. 16 including a loop and three different 3-vertices. The left most vertex of Fig. 16 is a

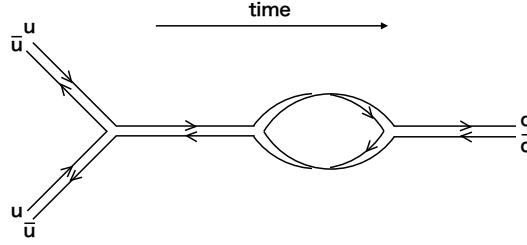


FIG. 16. The 1 loop diagram for $\bar{u}u + \bar{u}u \rightarrow \bar{d}d$ corresponding to (c) of Fig. 14.

meson-meson-meson where all mesons are the u type, as shown as (a) of Fig. 17. The middle and right most vertices are meson-baryon-baryon vertices, summarized as (b) and (c) of Fig. 17.

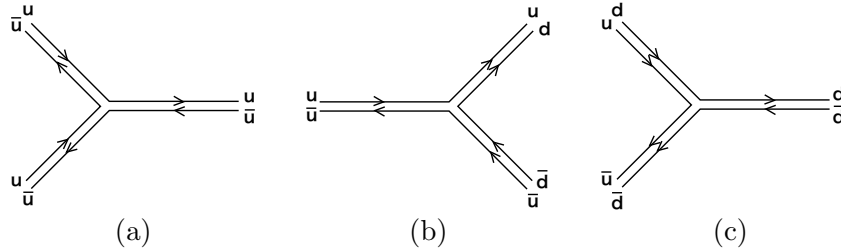


FIG. 17. The three 3-vertices included in the 1 loop diagram in Fig. 16. The time direction is from left to right.

Once we get these elementary vertices, it is easy for us to expect what kind of scatterings are possible without performing numerical simulations. Therefore, next our task is to track down all possible vertices. To this end, symmetry is helpful. Our system has the symmetry $F : \Psi_1 \leftrightarrow \Psi_2$ due to the special choice of the parameters given in Eq. (2). This ensures the “flavor” symmetry among the vortices as $F : (X_u(t), Y_u(t)) \leftrightarrow (X_d(t), Y_d(t))$, where $(X_{u,d}(t), Y_{u,d}(t))$ stands for the position of a u or d vortex at time t . Furthermore, the GP equations are

invariant under the time reversal symmetry $T : \Psi_i(x_1, x_2, t) \leftrightarrow \Psi_i^*(x_1, x_2, -t)$, and the parity transformation $P : \Psi_i(x_1, x_2, t) \leftrightarrow \Psi_i(x_1, -x_2, t)$. Note that the parity transformation in even spatial dimensions is identical to a reflection symmetry on an axis. With respect to the vortices, the former transforms a u vortex to a \bar{u} vortex as $T : (X_u(t), Y_u(t)) \leftrightarrow (X_{\bar{u}}(-t), Y_{\bar{u}}(-t))$. The same holds for d and \bar{d} vortices. Similarly, the latter also transforms a u vortex to \bar{u} since it exchanges $\theta = \arg(x_1 + ix_2) \leftrightarrow -\theta = \arg(x_1 - ix_2)$. Hence, the parity transformation is $P : (X_u(t), Y_u(t)) \leftrightarrow (X_{\bar{u}}(t), -Y_{\bar{u}}(t))$, and similar for d and \bar{d} vortices. By using the F , T , and P transformations, we can exhaust all possible diagrams as summarized in Fig. 18. For example, the diagrams labelled by (mddd1) and

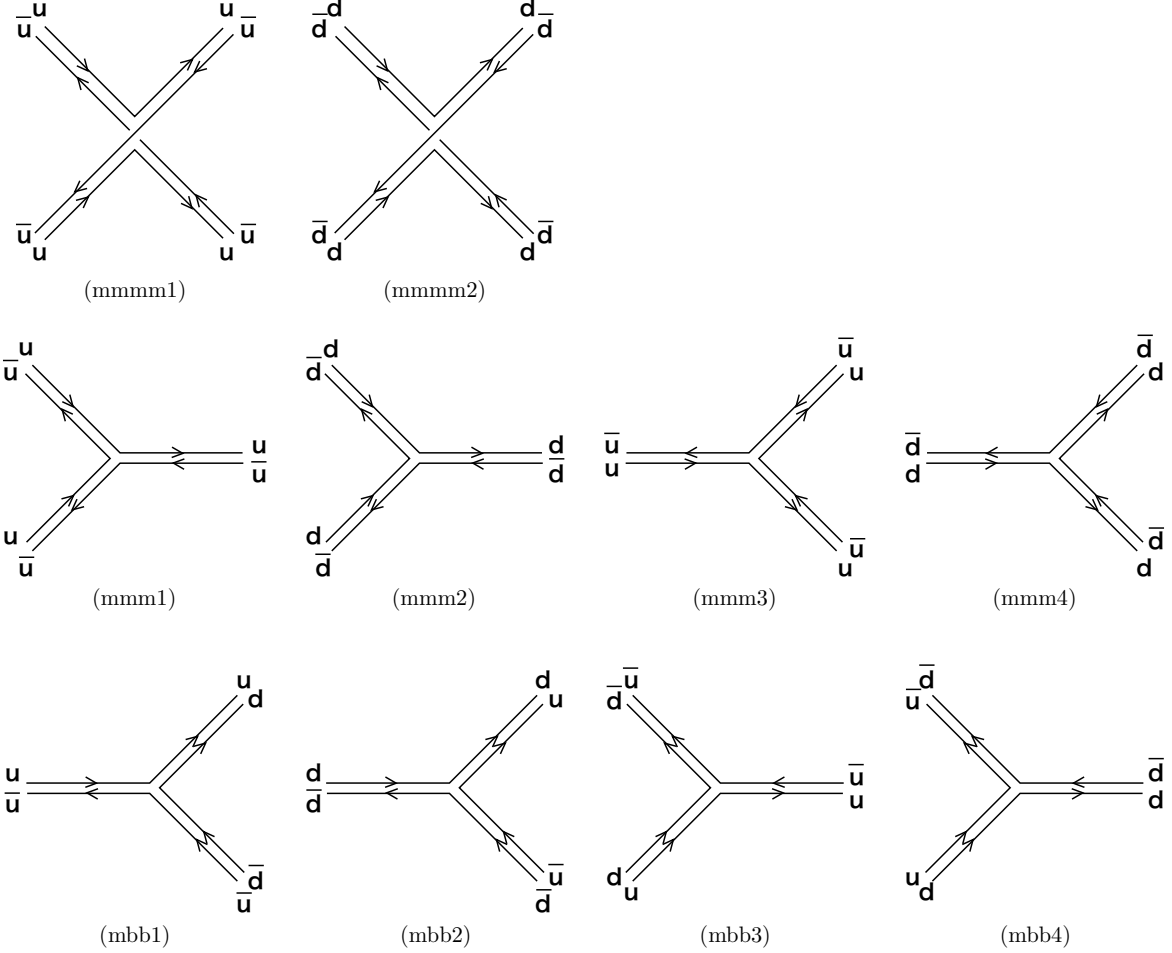


FIG. 18. Feynman diagrams found in two u (d) mesons scattering experiments. The first row shows the meson-meson-meson vertices. The second row shows the meson-meson-meson vertices, and the third row shows the meson-baryon-baryon vertices.

(mddd2) are exchanged by the F transformation, while those labelled by (mddd1) and (mddd3) are related by the T transformation. All the diagrams in Fig. 18 are invariant under the P transformation.

E. $\bar{u}u$ - $\bar{u}u$ collisions with impact parameters

The final process for the $\bar{u}u$ - $\bar{u}u$ collisions are scatterings with impact parameters. The initial mesons are placed at $(\tilde{x}_1, \tilde{x}_2) = (\pm\tilde{b}, 50)$. First, we horizontally shift the initial mesons of Fig. 6 by $\tilde{b} = 2.5$ as shown in Fig. 19. The scattering goes almost similarly to the head-on collision shown in Fig. 6 except for a scattering angle. As can be seen in the panel of $\tilde{t} = 100$ of Fig. 19, the new mesons created after the recombination are not vertical but diagonal.

As is naturally expected, the scattering angle gets smaller as the impact parameter becomes larger. Fig. 20 shows a scattering with impact parameter $\tilde{b} = 5$. Namely, the two mesons are not initially overlapped horizontally.

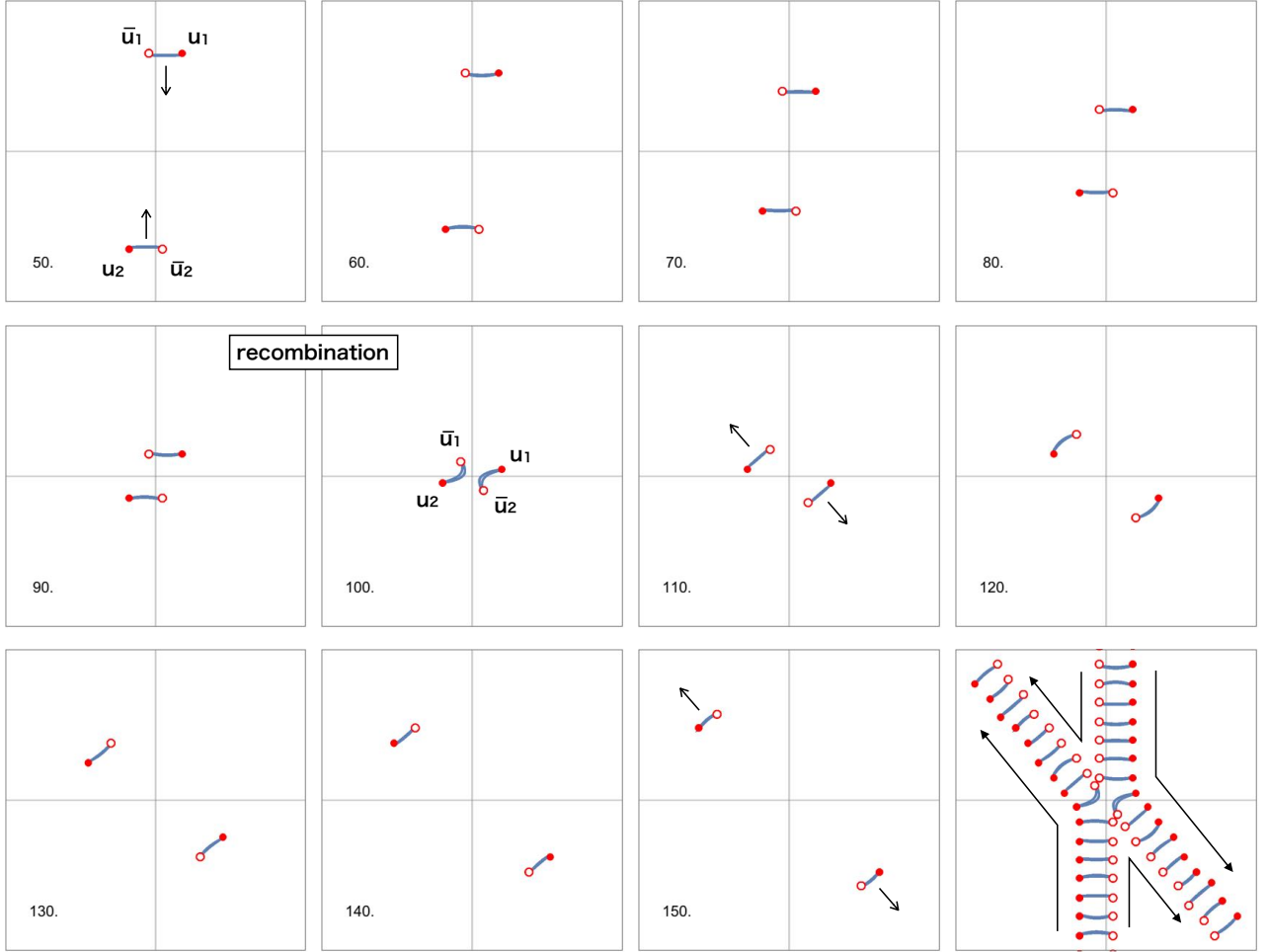


FIG. 19. Meson-meson scattering ($\bar{u}u - \bar{u}u$) with an impact parameter. Initially, the two mesons are placed at $(\tilde{x}_1, \tilde{x}_2) = (\tilde{b}, 50)$, and $(-\tilde{b}, 50)$ with the impact parameter $\tilde{b} = 2.5$. We show the snap shots with $\tilde{t} = 50 \sim 150$ with interval $\delta\tilde{t} = 10$. The panel at the right-bottom corner is a sequence photograph. The plot region is $\tilde{x}_{1,2} \in [-40, 40]$.

Nevertheless, the recombination occurs during the collision, and the mesons collide with a negative scattering angle.

If we put the initial mesons with a larger impact parameter, they pass through almost without interactions. Fig. 21 shows the scattering with the impact parameter $\tilde{b} = 7.5$. The mesons go almost straight with a negative but small scattering angle. This suggests that the asymptotic meson-meson interaction is attractive. We summarize the scatterings with impact parameters $\tilde{b} = 0, 2.5, 5$ and 7.5 in Fig. 22.

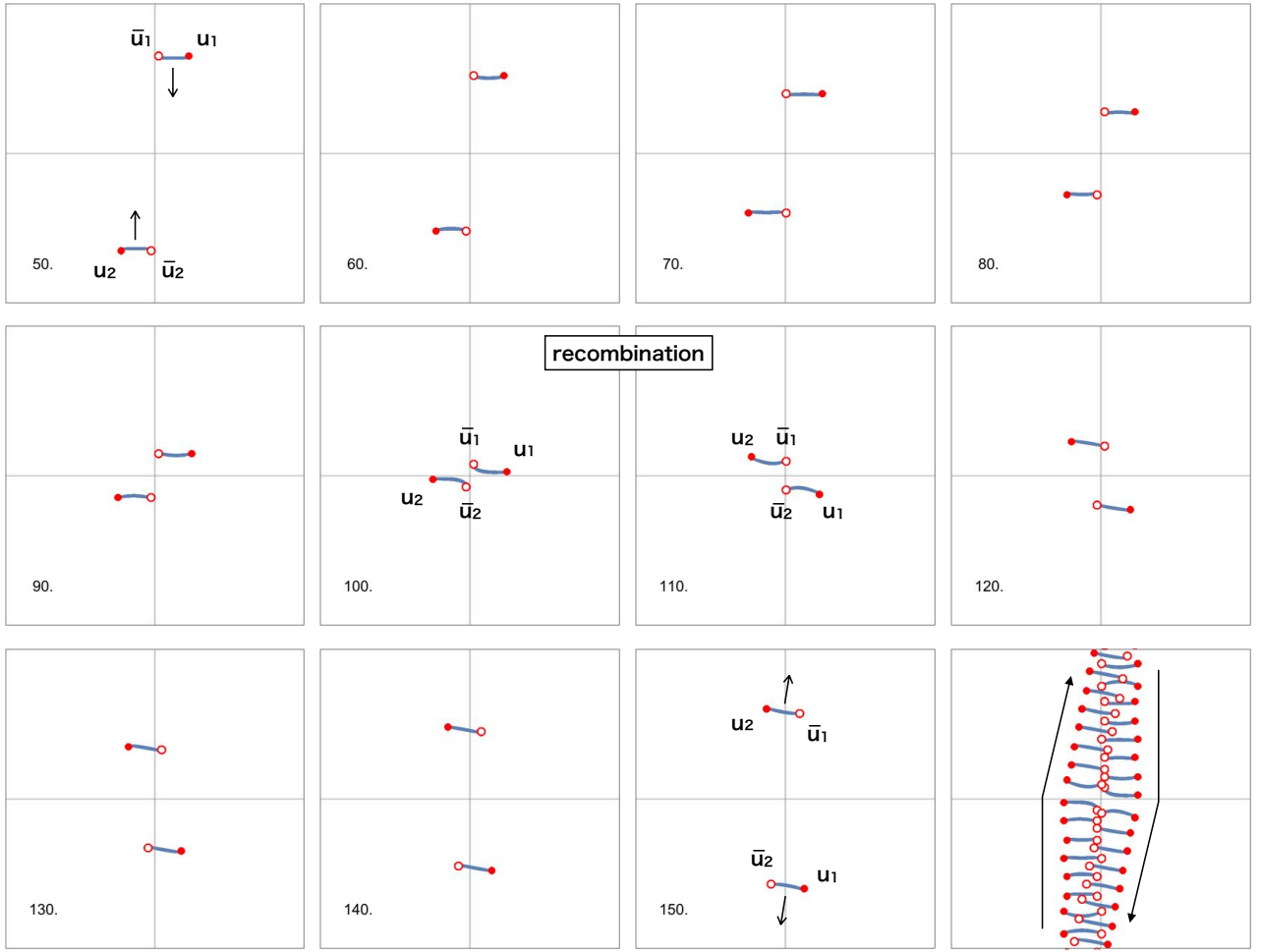


FIG. 20. Meson-meson scattering ($\bar{u}u-\bar{u}u$) with an impact parameter. Initially, the two mesons are placed at $(\tilde{x}_1, \tilde{x}_2) = (\pm\tilde{b}, 50)$ with the impact parameter $\tilde{b} = 5$. We show the snapshots with $\tilde{t} = 50 \sim 150$ with interval $\delta\tilde{t} = 10$. The panel at the right-bottom corner is a sequence photograph. The plot region is $\tilde{x}_{1,2} \in [-40, 40]$.

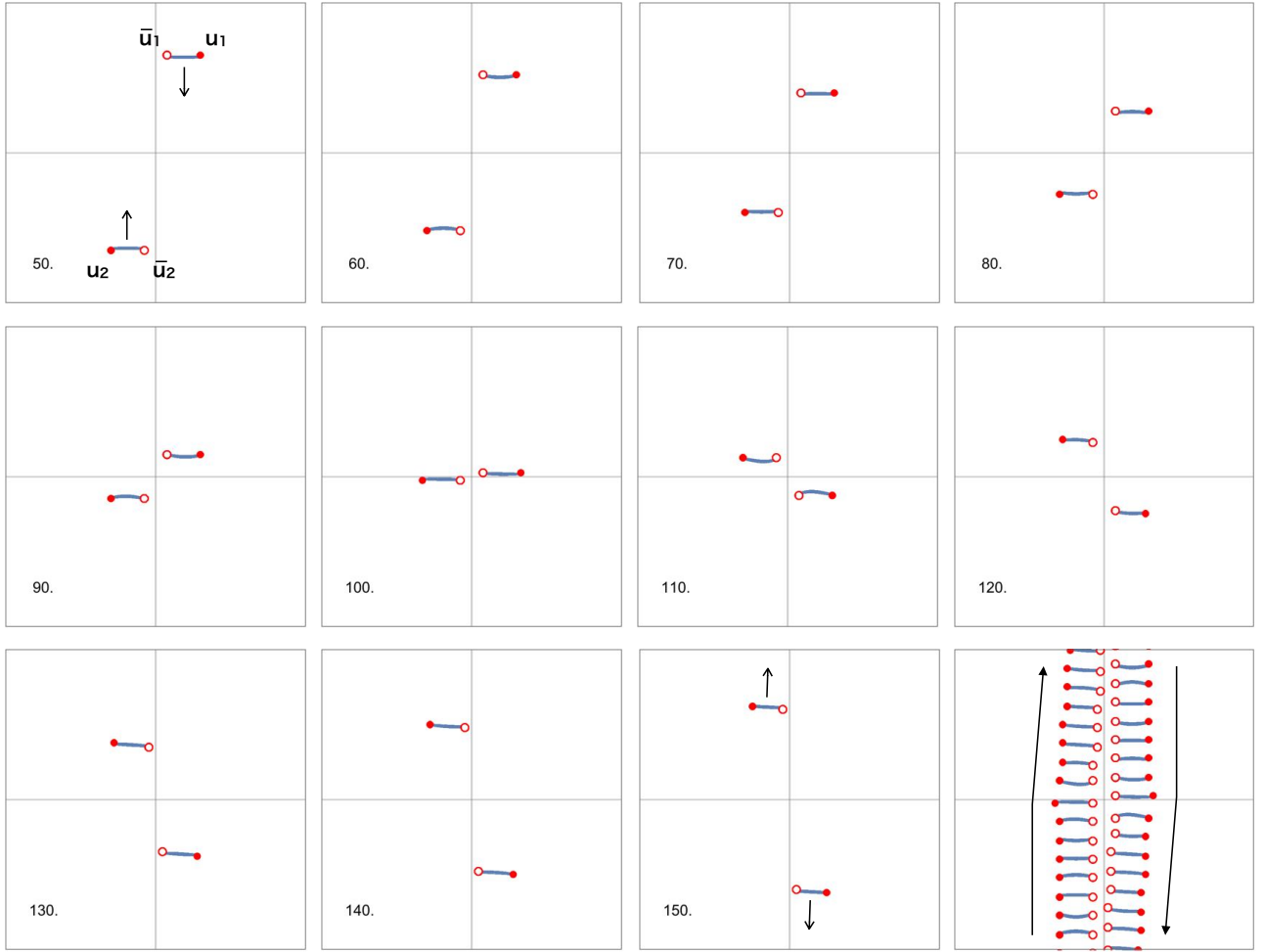


FIG. 21. Meson-meson scattering ($\bar{u}u\text{-}\bar{u}u$) with an impact parameter. Initially, the two mesons are placed at $(\tilde{x}_1, \tilde{x}_2) = (\pm\tilde{b}, 50)$ with the impact parameter $\tilde{b} = 7.5$. We show the snapshots with $\tilde{t} = 50 \sim 150$ with interval $\delta\tilde{t} = 10$. The panel at the right-bottom corner is a sequence photograph. The plot region is $\tilde{x}_{1,2} \in [-40, 40]$.

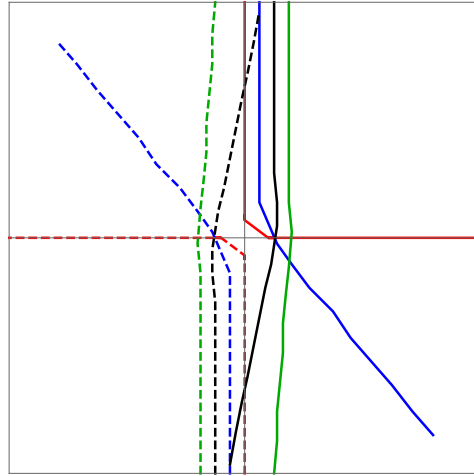


FIG. 22. The orbits of centers of the mesons during the meson-meson scatterings with the impact parameters $\tilde{b} = 0, 2.5, 5,$ and 7.5 corresponding to Figs. 6, 19, 20, and 21. The plotted region is $\tilde{x}_i \in [-40, 40]$.

IV. MESON-MESON SCATTERING: THE CASE OF $\bar{u}u\text{-}\bar{d}d$

A. $\bar{u}u\text{-}\bar{d}d$ head-on collision at 0 angle

Let us next study scatterings of a u meson and a d meson. We first collide the two mesons head-on. The initial configuration is prepared by superposing a u meson at $(\tilde{x}_1, \tilde{x}_2) = (0, 50)$ and the d meson at $(\tilde{x}_1, \tilde{x}_2) = (0, -50)$ [precisely speaking, we put a u vortex at $(\tilde{x}_1, \tilde{x}_2) = (5, 50)$ and a \bar{u} vortex at $(\tilde{x}_1, \tilde{x}_2) = (-5, 50)$, and a d vortex at $(\tilde{x}_1, \tilde{x}_2) = (-5, -50)$ and a \bar{d} vortex at $(\tilde{x}_1, \tilde{x}_2) = (5, -50)$]. The outlook of the scattering is shown in Fig. 23, which one might think is not so interesting compared to the $\bar{u}u\text{-}\bar{u}u$ head-on collision given in Fig. 5. Indeed, the two mesons

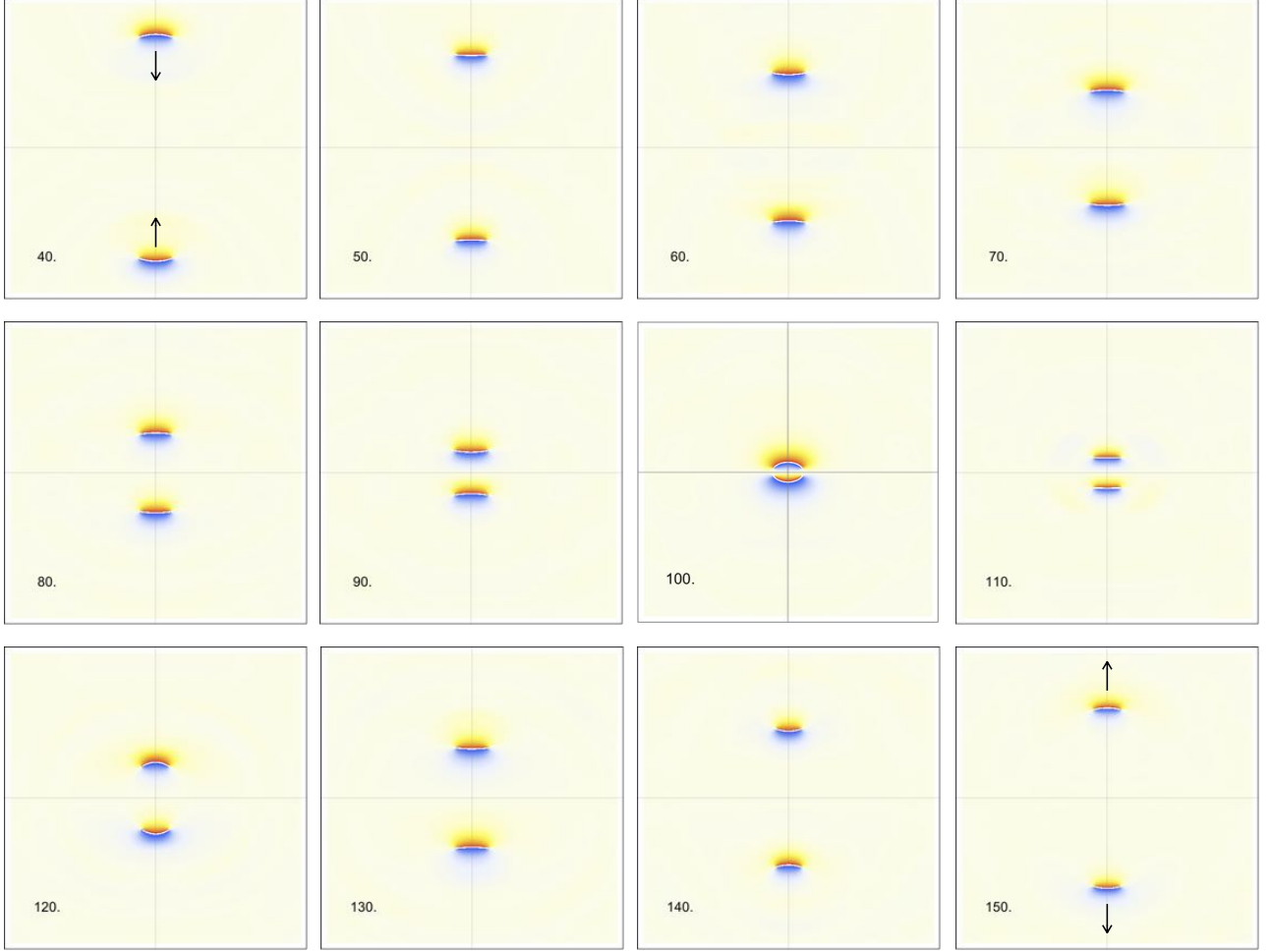


FIG. 23. The u and d meson scattering: Color density plots of the relative phase $\arg(\Psi_1) - \arg(\Psi_2)$. We initially ($\tilde{t} = 0$) set the u meson at $(\tilde{x}_1, \tilde{x}_2) = (0, 50)$, and the d meson at $(\tilde{x}_1, \tilde{x}_2) = (0, -50)$. They straightly run with almost constant speeds and pass through each other without an interaction. We show the snapshots from $\tilde{t} = 40$ to 150 with interval $\delta\tilde{t} = 10$, and the plot region is $\tilde{x}_{1,2} \in [-40, 40]$.

seem to pass through without an interaction, see Figs. 23 and 24. This observation is true if we look at only the vortices. However, it is not true for the SG solitons. As can be seen from Fig. 23, this scattering can be understood as a collision of one SG soliton (belonging to the u meson) and the other SG soliton (belonging to the d meson). This can be seen by noting that the color orders along the \tilde{x}_2 -axis are the same for the u and d mesons. This situation is in contrast to the meson-meson scattering in Fig. 5 in which the same species involve the SG and anti-SG solitons.

To see a nontrivial phenomenon in this scattering, let us carefully observe the period of passing. Fig. 25 shows snapshots in close-up at $\tilde{t} = 97.5, 100, 102.5, 105$. While the u and \bar{d} (d and \bar{u}) vortices pass through each other, the SG solitons largely bend toward the opposite direction compared to Fig. 7 due to repulsive interaction between the SG solitons. Thus, distance between two SG solitons at the center of mesons never vanish, and the SG solitons backscatter.

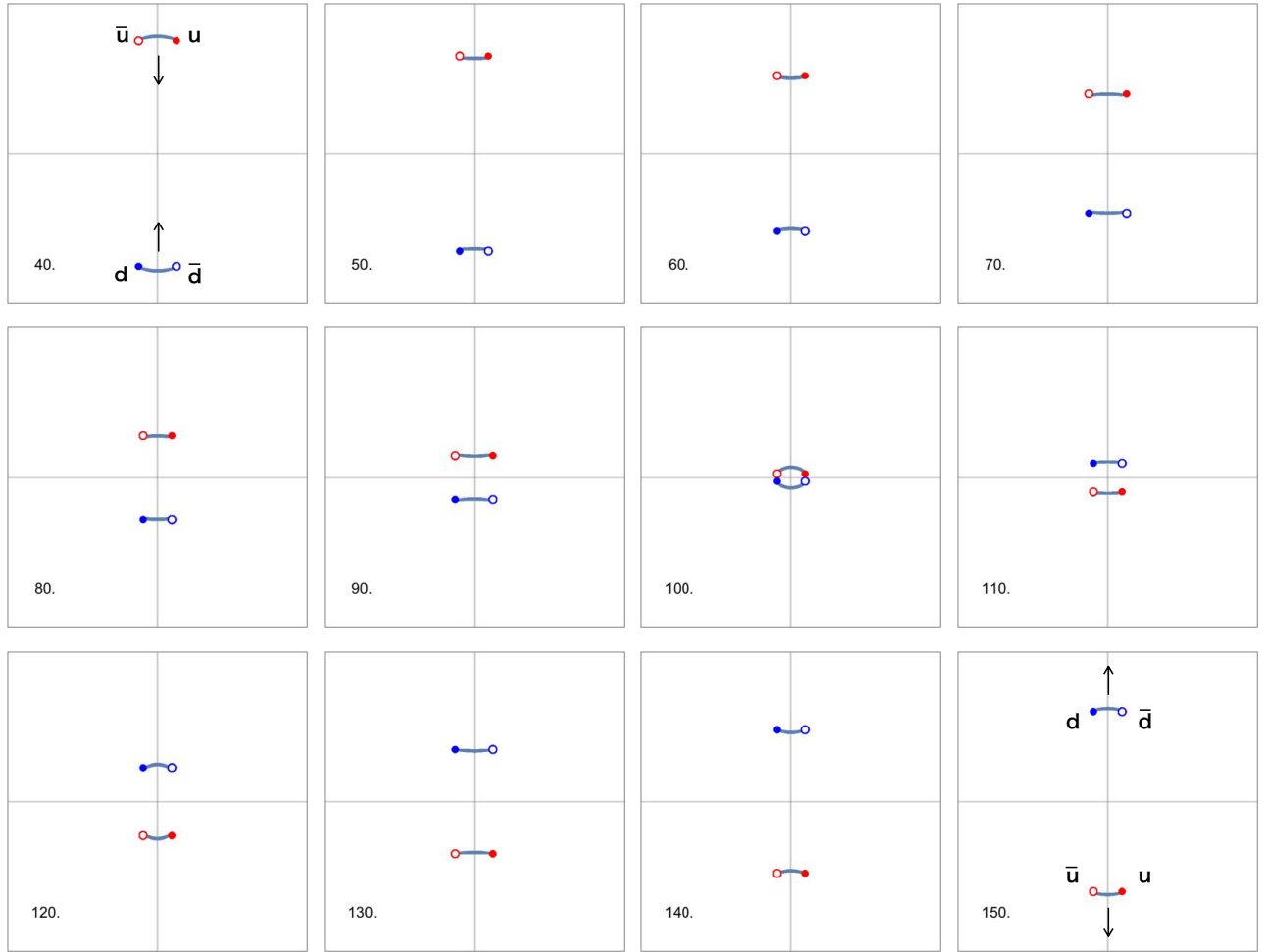


FIG. 24. A simplified plot of the u meson and d meson scattering shown in Fig. 23. We put painted red disks (unpainted red circle) at the points corresponding to the u (\bar{u}) vortex centers. Similarly, we put painted blue disks (unpainted blue circle) at the points corresponding to the d (\bar{d}) vortex centers. Gray regions bridging the u and \bar{u} vortices (d and \bar{d}) show the SG solitons. The gray regions are those where the relative phases take the values within $3 \leq |\arg(\Psi_1) - \arg(\Psi_2)| \leq \pi$.

Fig. 26 shows the relative phase $\arg(\Psi_1) - \arg(\Psi_2)$ on the \tilde{x}_2 axis. Throughout the scattering, there always exist two SG solitons (jumps from $-\pi \rightarrow \pi$). Since they are topologically protected, they cannot be annihilated. This is the reason why their distance does not vanish and they backscatter.

Thus, we found that the SG solitons backscatter whereas the vortices at the ends of mesons pass through. Along with this observation, we conclude that the mesons interchange the SG solitons before and after the head-on collision.

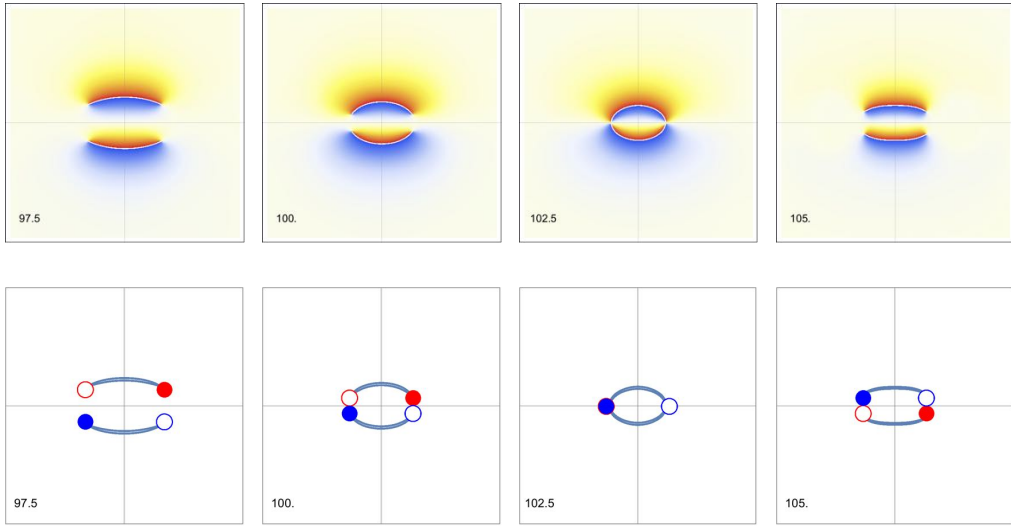


FIG. 25. Snapshots in close-up for $\hat{x}_i \in [-15, 15]$ at $\hat{t} = 97.5, 100, 102.5, 105$ for the u meson and d meson scattering given in Figs. 23 and 24. The SG solitons from the top and bottom gradually bend as they are close by and backscatter, whereas the vortices at the ends of the mesons pass through each other. Namely, the mesons interchange the SG solitons during the collision.

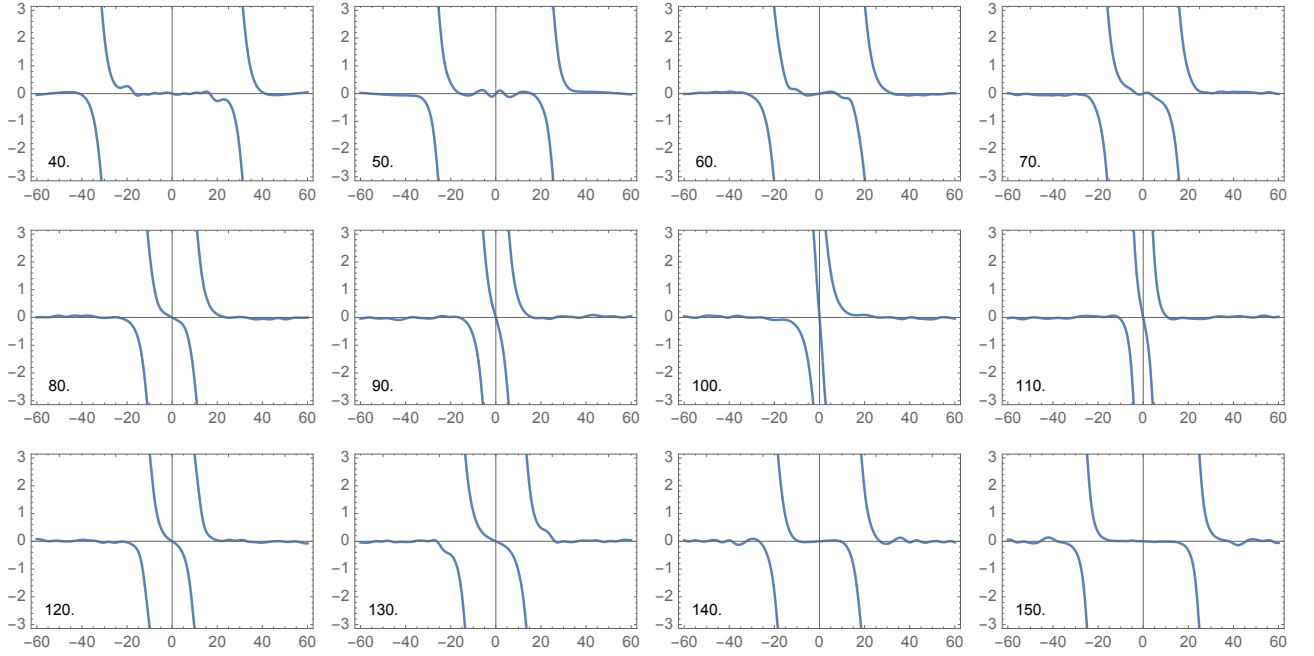


FIG. 26. The solid blue curve shows the relative phase $\arg(\Psi_1) - \arg(\Psi_2)$ along the \hat{x}_2 -axis of Fig. 23. The SG solitons coming from the right and left-hand sides collide and scatter backward. Throughout the scattering, the SG winding number ($= 2$) is preserved.

B. $\bar{u}u\text{-}\bar{d}d$ scattering at $\pi/8$ angle

The collision of the u and d mesons studied in the previous section is not so interesting in the sense that it does not include recombination phenomena which commonly occurs for the u and u meson scatterings. To see if the recombination is peculiar to the u and u meson scattering only or it is general for most scatterings, let us investigate the collision of the u and d mesons with angles here and in the next subsection.

Fig. 27 shows the outlook of the head-on collision of the u and d mesons with angle $\pi/8$. Compared to Fig. 9, the lower $\bar{u}u$ meson is replaced by $\bar{d}d$. At a first glance, the mesons seem to mere pass through each other, just as the

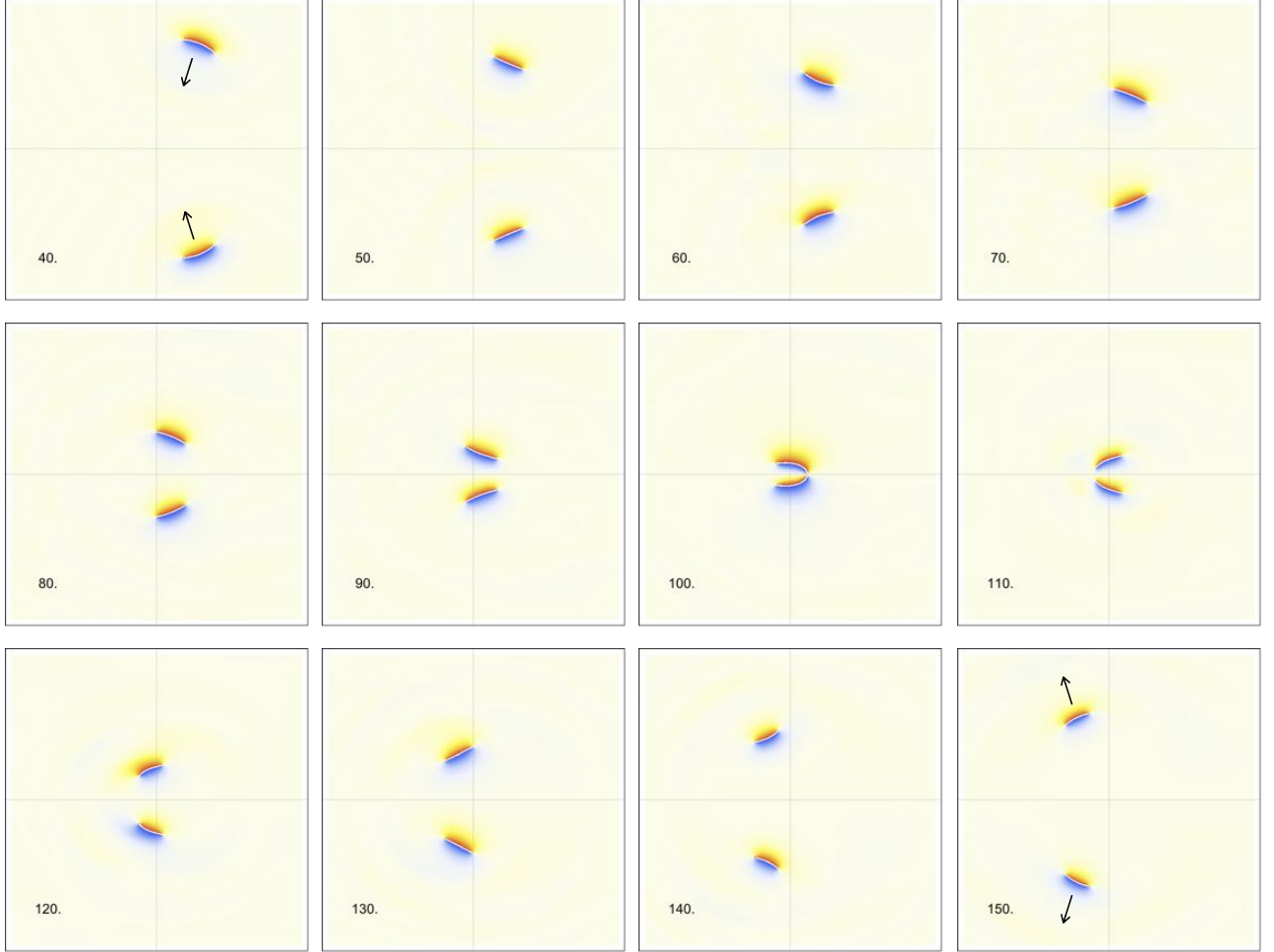


FIG. 27. Scattering of the slightly tilted u and d mesons with angle $\pi/8$. We initially ($\tilde{t} = 0$) set the u meson at $(\tilde{x}_1, \tilde{x}_2) = (50 \sin \pi/8, 50 \cos \pi/8)$, and the d meson at $(\tilde{x}_1, \tilde{x}_2) = (50 \sin \pi/8, -50 \cos \pi/8)$. We only show the snapshots from $\tilde{t} = 40$ to 150 with interval $\delta\tilde{t} = 10$, and the plot region is $\tilde{x}_{1,2} \in [-40, 40]$.

previous scattering in Fig. 23. However, it is not such trivial. Since the mesons are tilted, there is a certain period that the u-vortex at the lower edge of the u meson and the \bar{d} -vortex at the upper edge of the d meson exchange their positions, while the remaining constituent vortices are left to be unchanged, see the snapshot at $\tilde{t} = 100$ of Fig. 28. Soon after, the second passing of the remaining \bar{u} and d vortices follows, see the snapshot at $\tilde{t} = 110$ of Fig. 28. The interchange of constituent vortices is accompanied by the recombination of the SG solitons. The period between the first and the second recombinations, the molecules are not u and d mesons but the baryon ud and anti-baryon $\bar{u}\bar{d}$. Indeed, the SG solitons bridge the u and d vortices (\bar{u} and \bar{d} vortices) in the snapshot at $\tilde{t} = 100$ of Fig. 28.

Thus, the simulation here implies that the recombination can happen universally not only for the mesons of the same spices but also for the different spices. We have not observed the recombination in Fig. 23, just because the two mesons are finely tuned to be exactly parallel.

Let us cut out the period with created baryons and see their motion in more details. Fig. 29 shows snapshots in

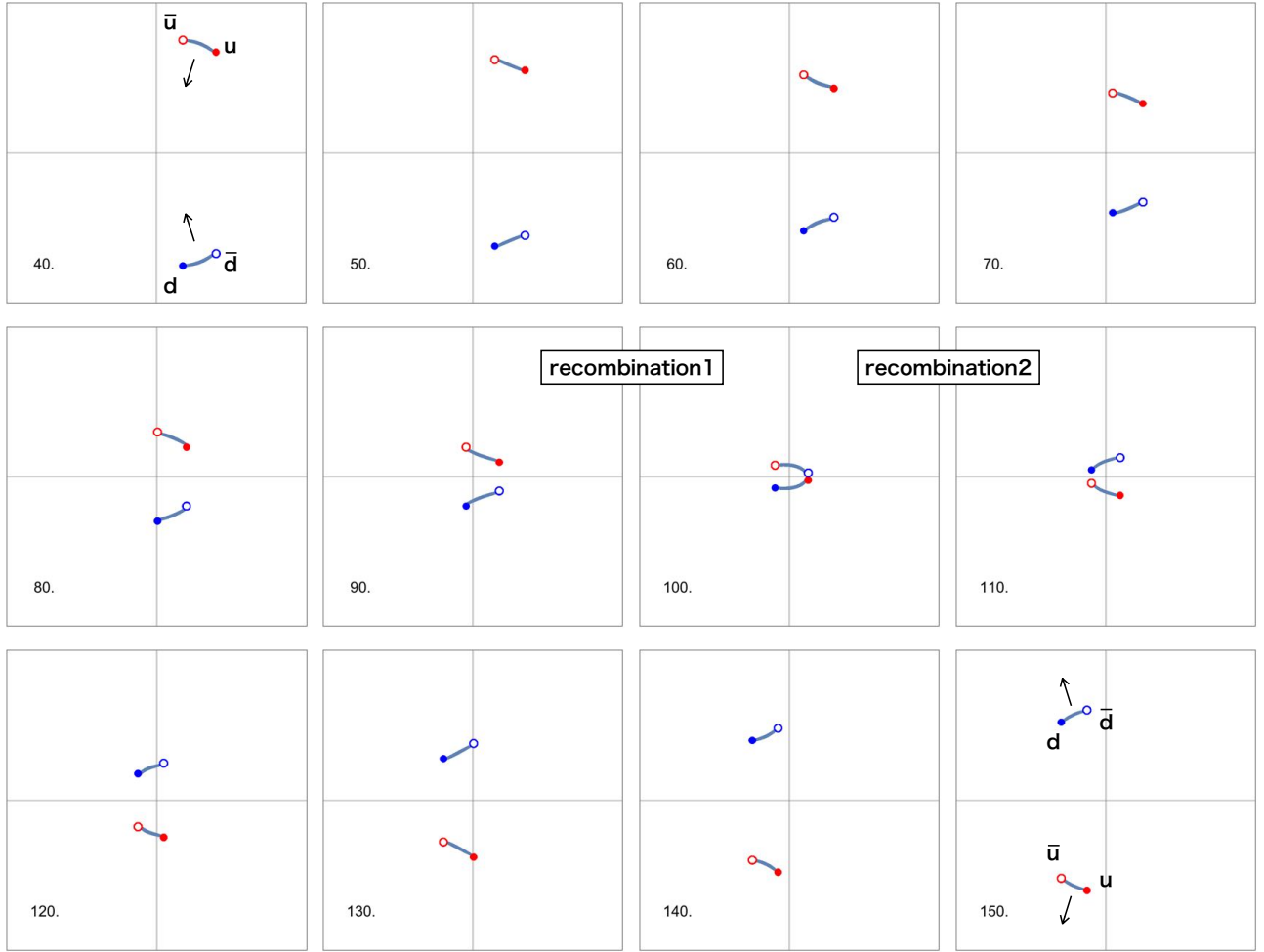


FIG. 28. A simplified plot of the u mesons scattering shown in Fig. 27.

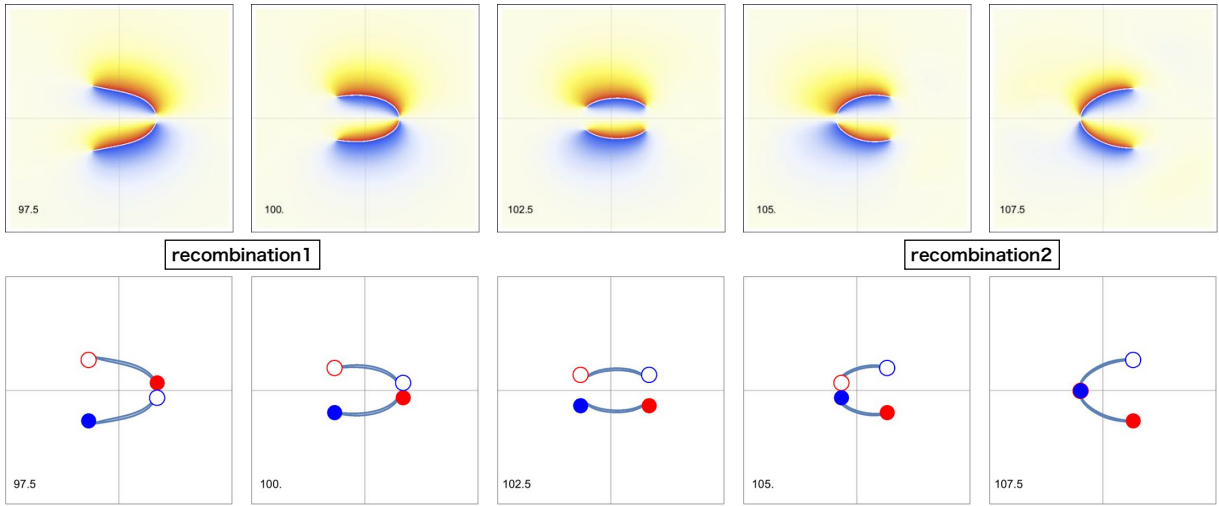


FIG. 29. Snapshots in close-up for $\tilde{x}_i \in [-15, 15]$ at $\tilde{t} = 97.5, 100, 102.5, 105, 107.5$ for the u meson and d meson scattering given in Figs. 27 and 28. The mesons are converted into the baryon and anti-baryon pair for a short period.

close-up for $\tilde{x}_i \in [-15, 15]$ at $\tilde{t} = 97.5, 100, 102.5, 105,$ and 107.5 . The baryon (anti-baryon) formed after the first recombination rotates counterclockwise (clockwise) until they are reformulated back into the mesons. During the period with baryons, they almost do not run. As a consequence, the meson orbits before and after the collision slightly shift due to delay of forming baryons.

C. $\bar{u}u\text{-}\bar{d}d$ scattering at $\pi/4$ angle

The observations in the previous subsection can be more sharply seen in the scattering of the u and d mesons with larger angle; we take $\pi/4$ here as an example. Fig. 30 shows an outlook of the scattering process. Qualitatively, it goes very similarly to that with the angle $\pi/8$ given in Fig. 28. Namely, the incoming u and d mesons are converted to the

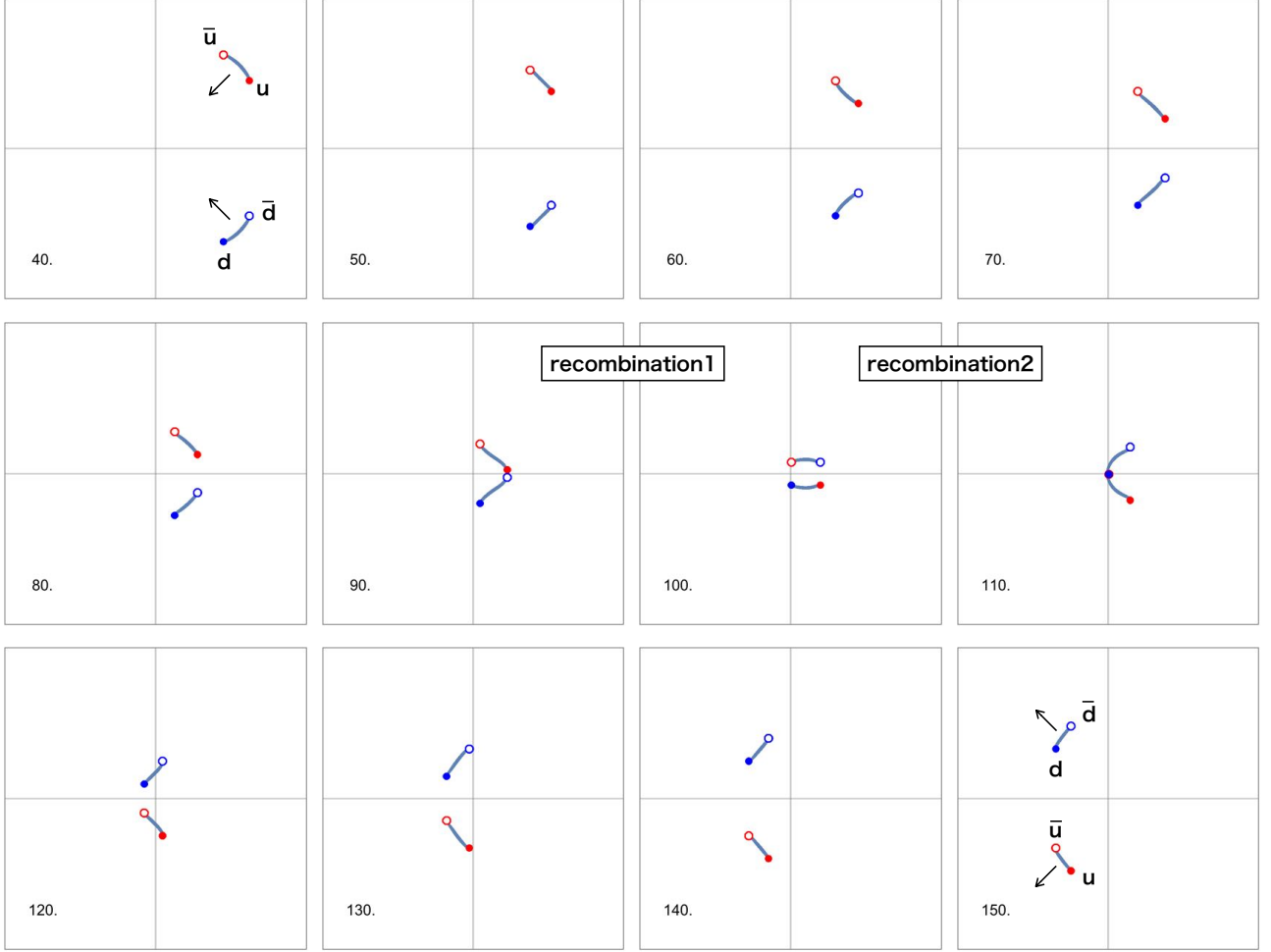


FIG. 30. Scattering of the tilted u and d mesons with angle $\pi/4$. We initially ($\tilde{t} = 0$) set the u meson at $(\tilde{x}_1, \tilde{x}_2) = (50 \sin \pi/4, 50 \cos \pi/4)$, and the d meson at $(\tilde{x}_1, \tilde{x}_2) = (50 \sin \pi/4, -50 \cos \pi/4)$. We only show the snapshots from $\tilde{t} = 40$ to 150 with interval $\delta\tilde{t} = 10$, and the plot region is $\tilde{x}_{1,2} \in [-40, 40]$.

intermediate baryon and anti-baryon pair at the first recombination. The baryons rotate at their position without run for a while. Then they are reformed back into the mesons at the second recombination and run straight toward the boundary. The baryonic period in this scattering is longer than the previous one because of the steeper angle of the incoming mesons. Comparing Figs. 29 and 31, the baryonic period is $\tilde{t} \simeq 97.5\text{-}105$ for the former while $\tilde{t} \simeq 95\text{-}107.5$ for the latter. A longer lifetime of the baryonic period makes the rotation of the baryons clearer to be seen.

As mentioned above, the conversion of mesons to baryon and anti-baryon results in delay of the straight orbits of the incoming and outgoing mesons. In order to see the delay clearer, we show sequence photographs for the u and d meson scatterings with $\pi/8$ and $\pi/4$ angles in Fig. 32. One can see the orbits of the constituent vortices steeply

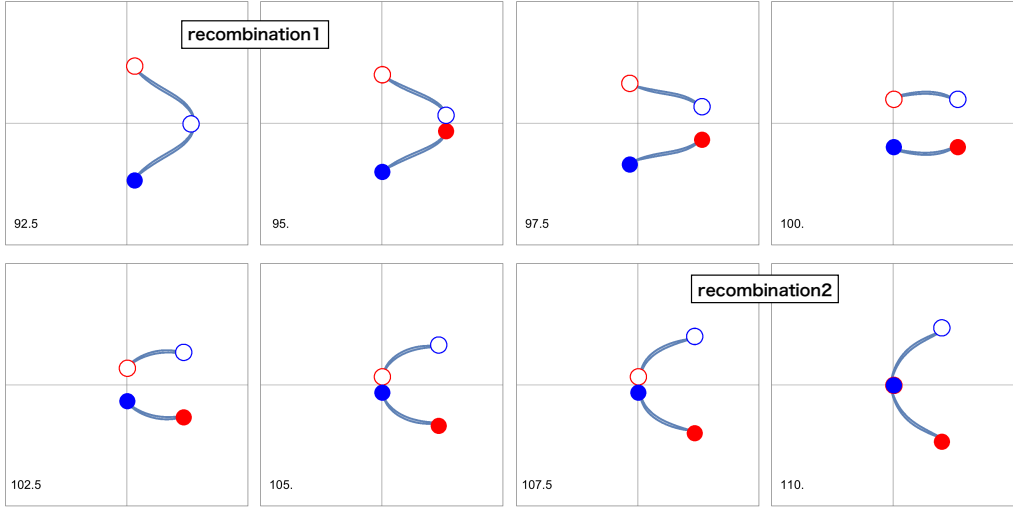


FIG. 31. Snapshots in close-up for $\tilde{x}_i \in [-15, 15]$ at $\tilde{t} = 92.5, 95, 97.5, 100, 102.5, 105, 107.5, 110$ for the u meson and d meson scattering given in Fig. 30.

bend at the timing of recombinations. Since vertical motions of the vortices in Fig. 32 are simple shift with almost constant speed, we can approximately regard the vertical axis as the time. Then the horizontal motions would remind us a phase shift which commonly appears in soliton scatterings or particle scattering. The phase shift in our system is due to the formation of unstable intermediate baryonic states with finite life time. It is interesting that a phase shift common for scattering is observed here, although the mechanism is peculiar to our system and has never been seen elsewhere.

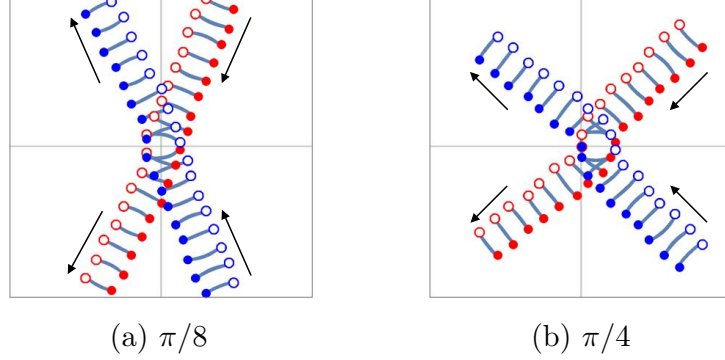


FIG. 32. Sequence photographs for the u and d meson scatterings with $\pi/8$ and $\pi/4$ angles given in Figs. 28 and 30.

D. Interaction vertices and Feynman diagrams

As in the u and u mesons scattering, we can describe the u and d mesons scattering by the Feynman diagram. The diagram for Fig. 32 is a 1-loop diagram given in Fig. 33 (a). It includes meson-meson-baryon-baryon vertices which are shown in Fig. 33 (b) and (c). They are invariant under the F and P transformations while they are exchanged by the T transformation. Hence, no more diagrams are generated by the symmetries.

Related to these meson-meson-baryon-baryon vertices, we observed in our previous work Ref. [16] that a long meson disintegrates into three short molecules as

$$\bar{u}u \rightarrow ud + \bar{d}d + \bar{d}\bar{u}. \quad (22)$$

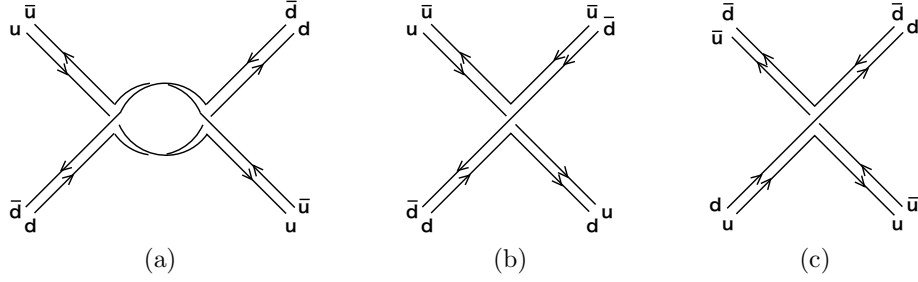


FIG. 33. (a) the Feynman diagram corresponding to the real processes in Fig. 30. (b) and (c) shows the meson-meson-baryon-baryon vertices which are building blocks of the twig diagram (a).

The Feynman diagrams corresponding to this and other related diagrams via the F , T , and P symmetries are given in Fig. 34. Interestingly, these diagrams can be generated by horizontally flipping an external leg of the diagrams (b) and (c) of Fig. 33. In a usual relativistic quantum field theory, the presence of the vertex (b) of Fig. 33 immediately means

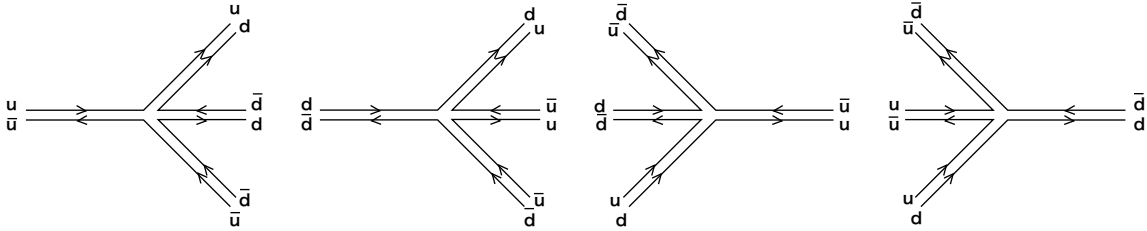


FIG. 34. The meson-meson-baryon-baryon vertices correspond to and relate to a long meson disintegration into a baryon, an anti baryon, and a meson.

that the vertex of the left-most panel of Fig. 34 also exists as either a real or virtual process. However, our theory here is not relativistic, and moreover we are dealing with only real processes which are solution of the GP equations. Therefore, for our system, the vertex (b) of Fig. 33 does not automatically ensure the vertex of the left-most panel of Fig. 34. We should emphasize that we put the four diagrams of Fig. 34 in our list of the real processes because we found them in real dynamics. To make contrast clearer, let us mention another process which we previously encountered in Refs. [14, 16]:

$$ud \rightarrow ud + \bar{d}\bar{u} + ud. \quad (23)$$

The corresponding Feynman diagram and the other diagrams obtained via the F , T , and P transformations are given in Fig. 35. By flipping the out-going external ud leg of the left-most diagram in Fig. 35, we can generate the diagram

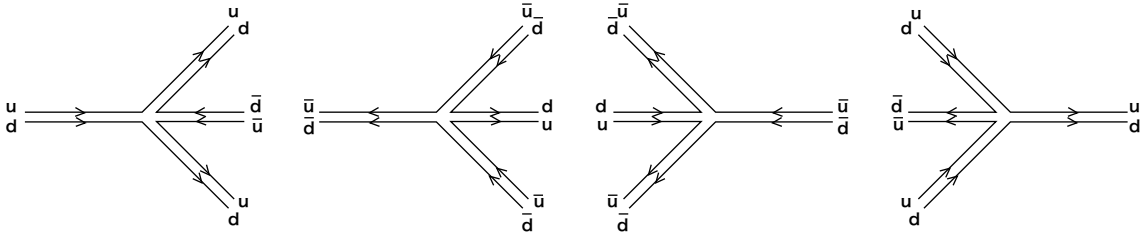


FIG. 35. The baryon-baryon-baryon-baryon vertices correspond to and relate to a long baryon disintegration into two baryons and one anti-baryon.

shown in the left panel of Fig. 36. However, a real process corresponding to this diagram does not seem to happen. This is because a baryon ud and an anti baryon $\bar{u}\bar{d}$ are a pair of the integer vortex and anti-vortex, so that they move

parallel with their distance being kept constant, as can be seen in the right panel of Fig. 36. Hence, we have learned that we cannot freely flip any external legs of a vertex from left (right) to right (left).

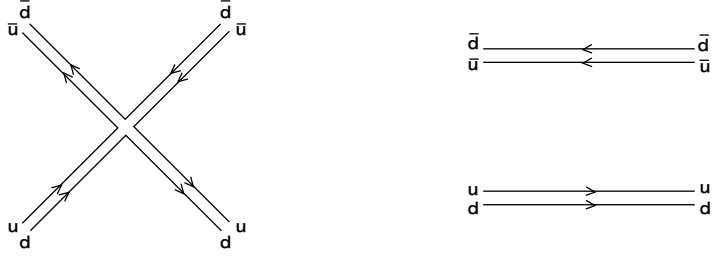


FIG. 36. The baryon-baryon-baryon-baryon vertices correspond to and relate to a long baryon disintegration into two baryons and an anti baryon.

E. $\bar{u}u\text{-}\bar{d}d$ collisions with impact parameters

To make our study self-contained, let us repeat the same simulations for $\bar{u}u$ and $\bar{d}d$, as those for $\bar{u}u$ and $\bar{u}u$ in Sec. III E. Namely, we study the u and d mesons collisions with the impact parameter \tilde{b} . As counterparts of Figs. 19, 20, and 21, we do the same simulations by replacing the lower $\bar{u}u$ meson with the $\bar{d}d$. The results are shown in Figs. 37, 38, and 39. Comparing Figs. 21 and 39, it turns out that the asymptotic interaction between the u and d mesons are much smaller than the one between the u and u mesons. Therefore, we see that the contact interaction dominates for the former.

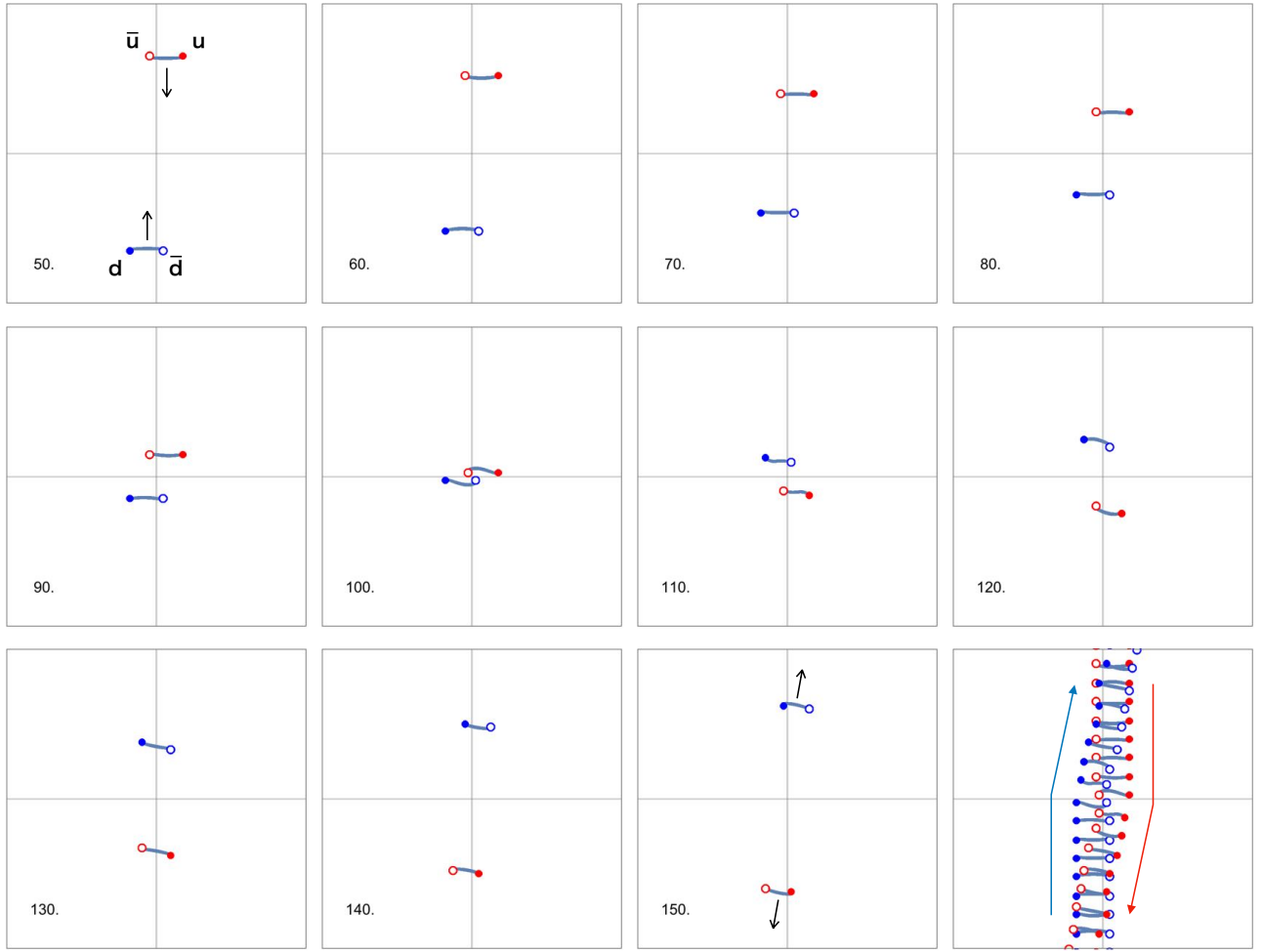


FIG. 37. Initial configuration is the same as that in Fig. 19 except for the fact that the lower meson is not $\bar{u}u$ but $\bar{d}d$. The plot region is $\tilde{x}^i \in [-40, 40]$ and $\tilde{b} = 2.5$.

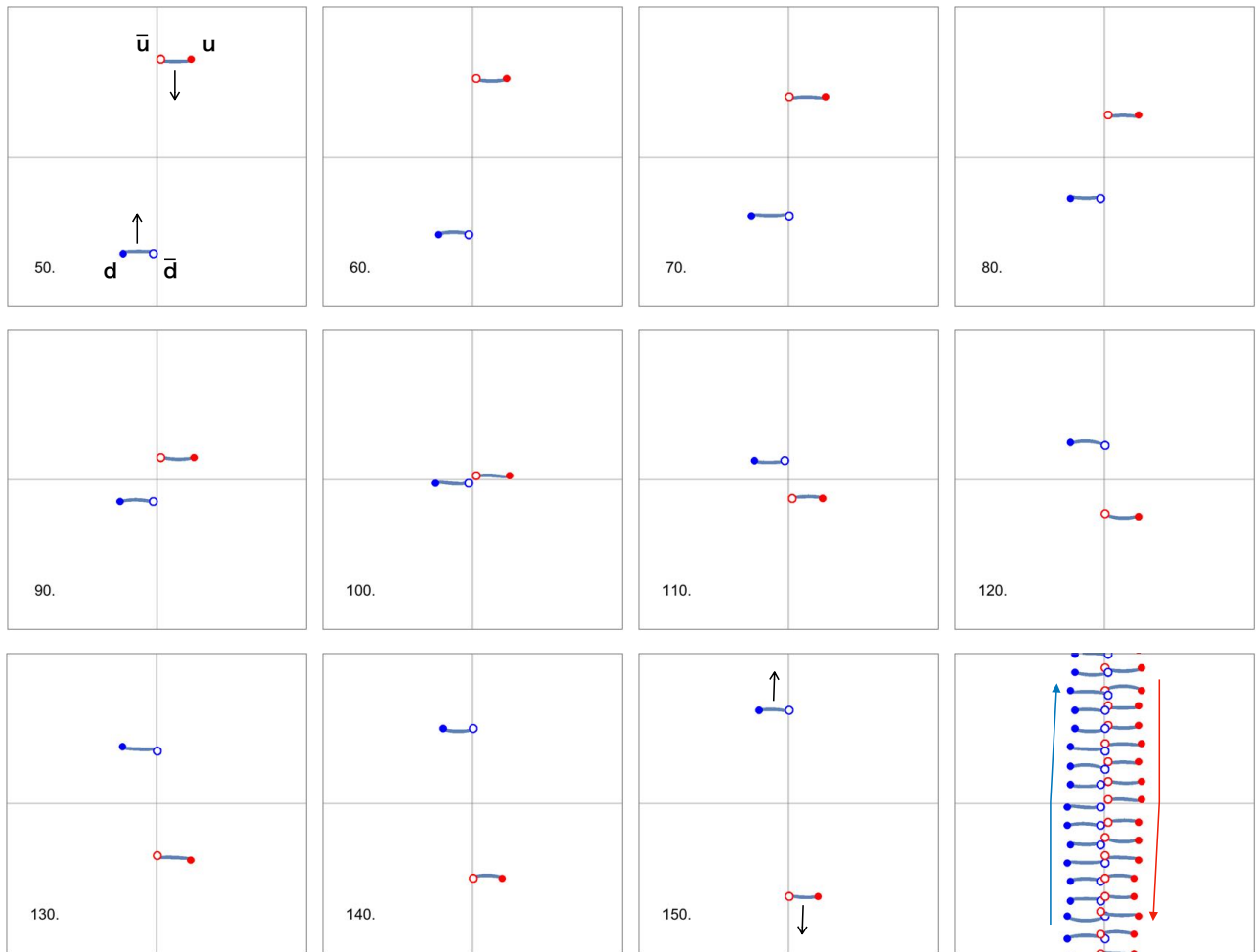


FIG. 38. Initial configuration is the same as that in Fig. 20 except for the fact that the lower meson is not $\bar{u}u$ but $\bar{d}d$. The plot region is $\tilde{x}^i \in [-40, 40]$ and $\tilde{b} = 5$.

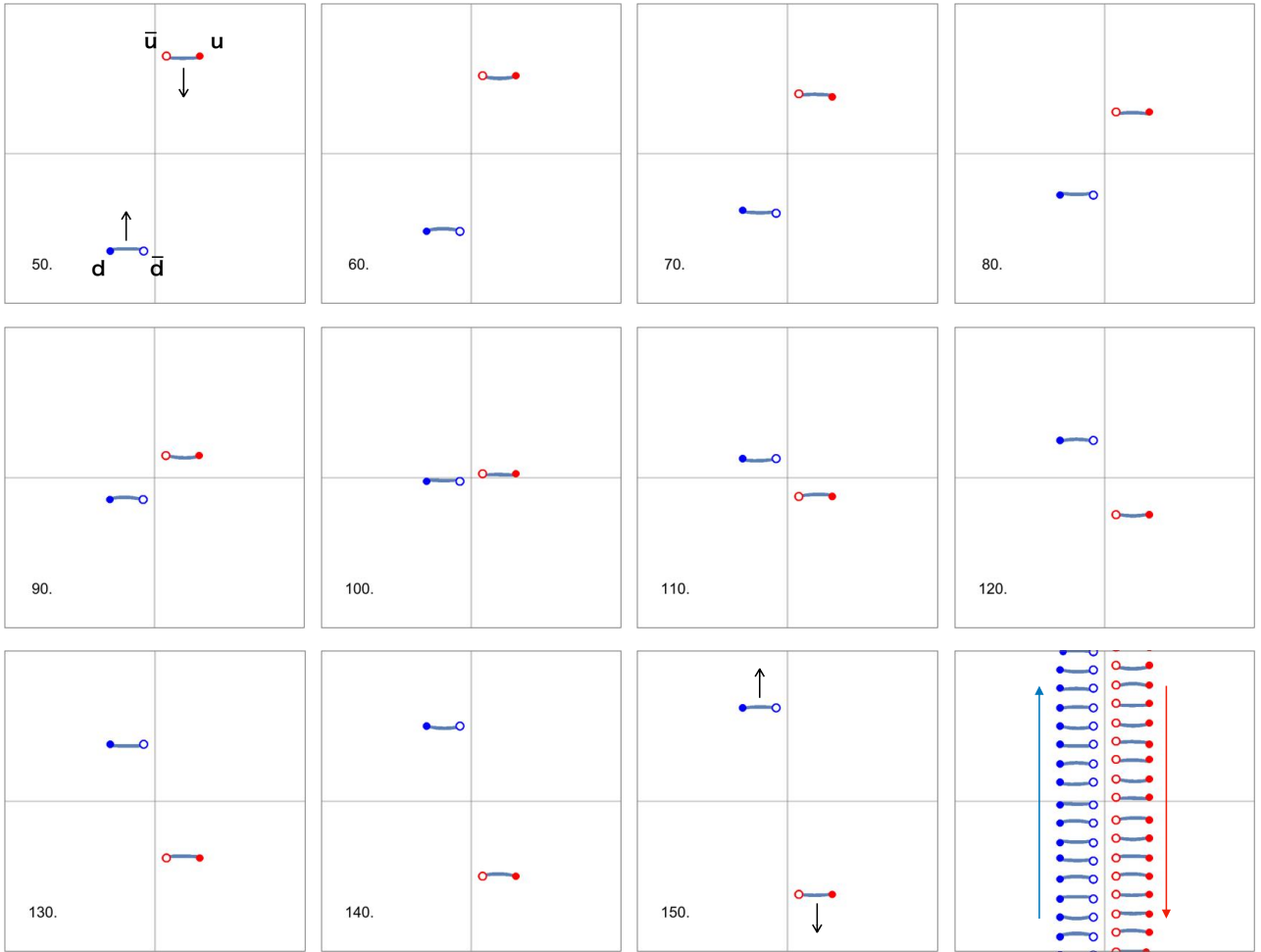


FIG. 39. Initial configuration is the same as that in Fig. 21 except for the fact that the lower meson is not $\bar{u}u$ but $\bar{d}d$. The plot region is $\tilde{x}^i \in [-40, 40]$ and $\tilde{b} = 7.5$.

V. BARYON-MESON SCATTERING

Our final vortical collider simulations are scatterings of a meson and a baryon. Since baryons do not run but rotate, we put a baryon at the origin as a target. Then, we put an incoming meson sufficiently far from the target baryon, and they collide quite similar to usual collider experiments. As expected, details of the scatterings sensitively depend on the timings of collision, namely geometric information such as relative positions and angles of the baryon and meson. It is impossible to simulate all cases, and so we introduce two typical scatterings which illustrate general features. In addition, we exhibit one more example which has a special phenomenon, a jet, which remind us hadron collider experiments.

A. Typical collisions

In this subsection, we exhibit two scattering simulations whose initial configurations are given in Fig. 40 (a) and (b). For both, we put the same meson as the one given in Fig. 4 at $(\tilde{x}_1, \tilde{x}_2) = (50, 0)$. Similarly, the same baryon as the one given in Fig. 4 is located at the origin. The meson runs toward the target baryon rotating at the origin. The difference between Fig. 40 (a) and (b) is that the initial angles of the target baryon are different by 180 degree, so that relative positions of the meson and baryon at the moment of collision are different.

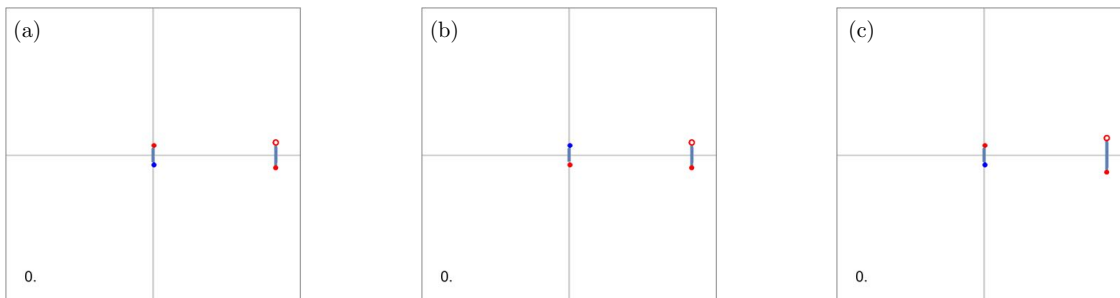
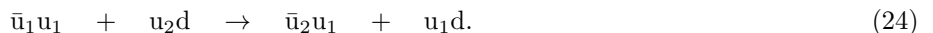


FIG. 40. The three initial configurations for a u meson and a baryon (ud) scattering. The displayed region is $\tilde{x}_i \in [-60, 60]$. The meson is placed at $(\tilde{x}_1, \tilde{x}_2) = (50, 0)$ and the target baryon is at the origin.

In Fig. 41, the scattering from the initial configuration in Fig. 40 (a) is shown. The u meson approaches the rotating target baryon and they collide. After the collision, a u meson runs toward a direction with a scattering angle about 45 degree while the baryon is left near the origin. Thus, what happens is just $\bar{u}u + ud \rightarrow \bar{u}u + ud$, and one might find nothing interesting for this process. However, as the case of the meson-meson scatterings, it is not so simple. One of nontrivial phenomena is the recombination before and after the collision. As can be seen in the panels with the time stamps $\tilde{t} = 90$ and 100, the meson and baryon exchange the u constituent vortices. Therefore, both the meson and baryon after the collision are different from those before the collision. If we express the initial meson as $\bar{u}_1 u_1$ and the initial baryon as $u_2 d$, the process can be summarized as the following vortical reaction



To see this better, let us carefully look at the collision period. Fig. 42 shows snapshots in close-up for $\tilde{x}_i \in [-15, 15]$ around the collision. We find that the snapshots are qualitatively the same as those given in Fig. 7 for the $\bar{u}u$ - $\bar{u}u$ scattering. As before, the recombination takes place together with partial annihilation of the SG and anti-SG solitons.

The other scattering from the initial configuration Fig. 40 (b) is also shown in Fig. 43. The scattering goes almost the same as the previous one. The u meson collides with the target baryon, and a u meson is scattered while a baryon is left near the origin. The scattering angle is now about -45 degree. The difference of the scattering angles is just due to the relative position and angle of the meson and baryon at the moment of the collision. Similarly to the first simulation, the meson and baryon experience the recombination once during the collision. Therefore, the vortical reaction is the same as Eq. (24). Nevertheless, detail dynamical processes of the recombination are not same. To see the difference clearer, let us zoom in on the collision moment shown in Fig. 44. On contrary to the previous case, the collision is accompanied not by the SG and anti-SG solitons but the SG and SG solitons. Hence, the recombination here is very similar to what we saw in Fig. 25 for the $\bar{u}u$ and $\bar{d}d$ meson scattering. Since the two SG solitons repel each other, they cannot be close. Only one set of the edges of the meson and baryon come across to exchange \bar{u}_1

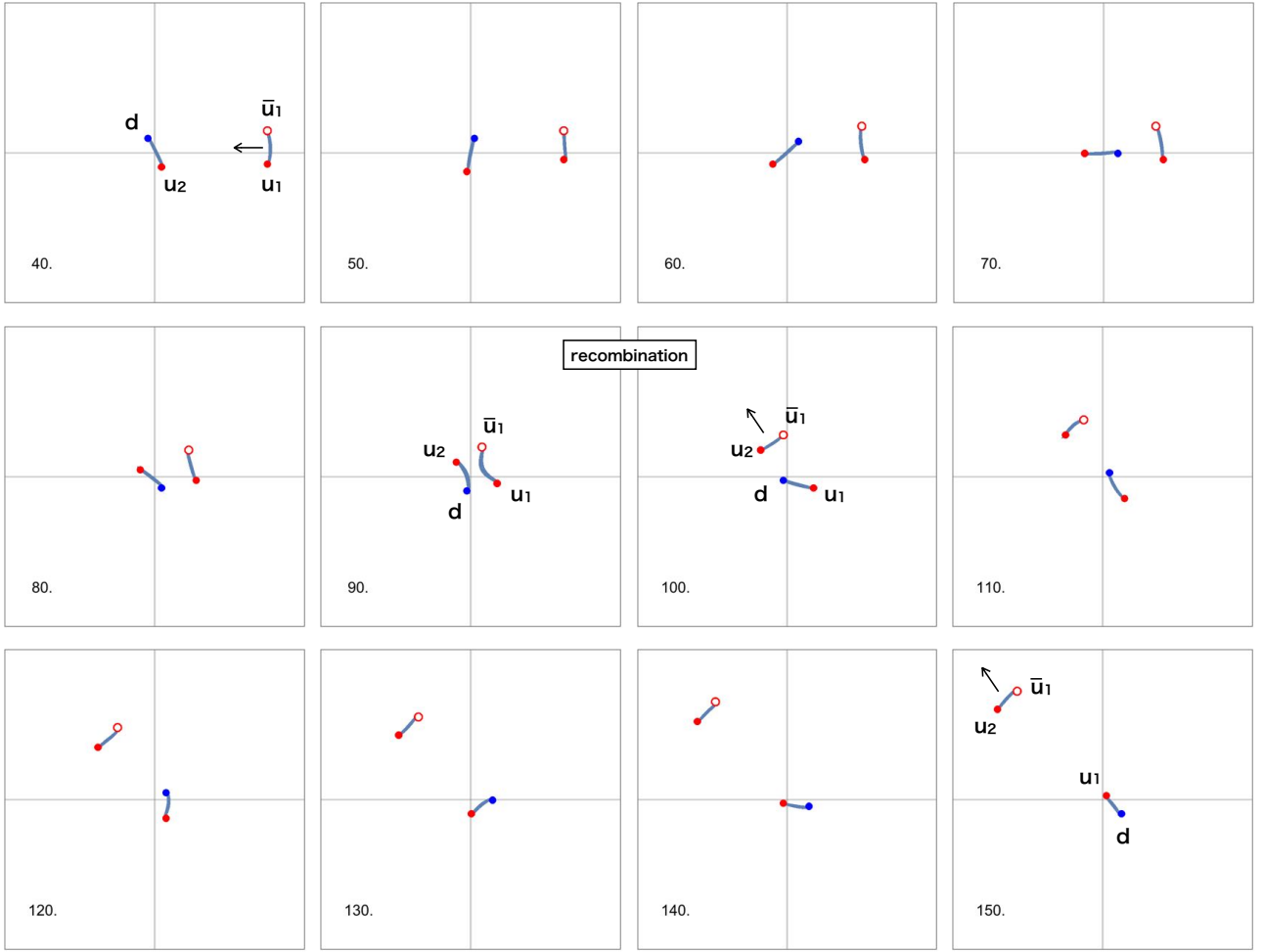


FIG. 41. The scattering of the meson $\bar{u}_1 u_1$ and the baryon $u_2 d$ with the initial configuration given in Fig. 40 (a). The collision accompanies the recombination at about $\tilde{t} = 90$. The outgoing meson is $\bar{u}_1 u_2$ and the new baryon $u_1 d$ is left near the origin. We show the snapshots from $\tilde{t} = 40$ to 150 with interval $\delta\tilde{t} = 10$, and the plot region is $\tilde{x}_{1,2} \in [-40, 40]$.

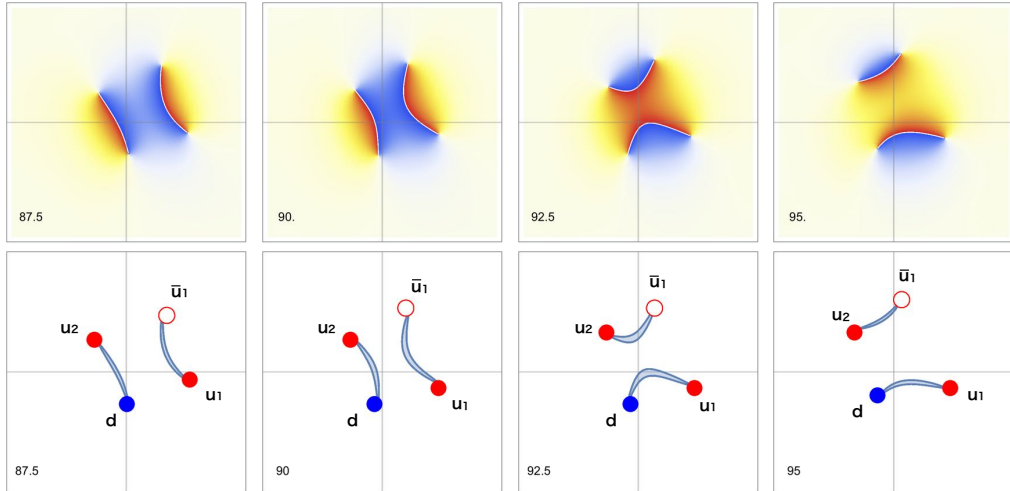


FIG. 42. Snap shots of Fig. 41 in close-up for $\tilde{x}_i \in [-15, 15]$ at $\tilde{t} = 87.5, 90, 92.5, 95$ are shown.

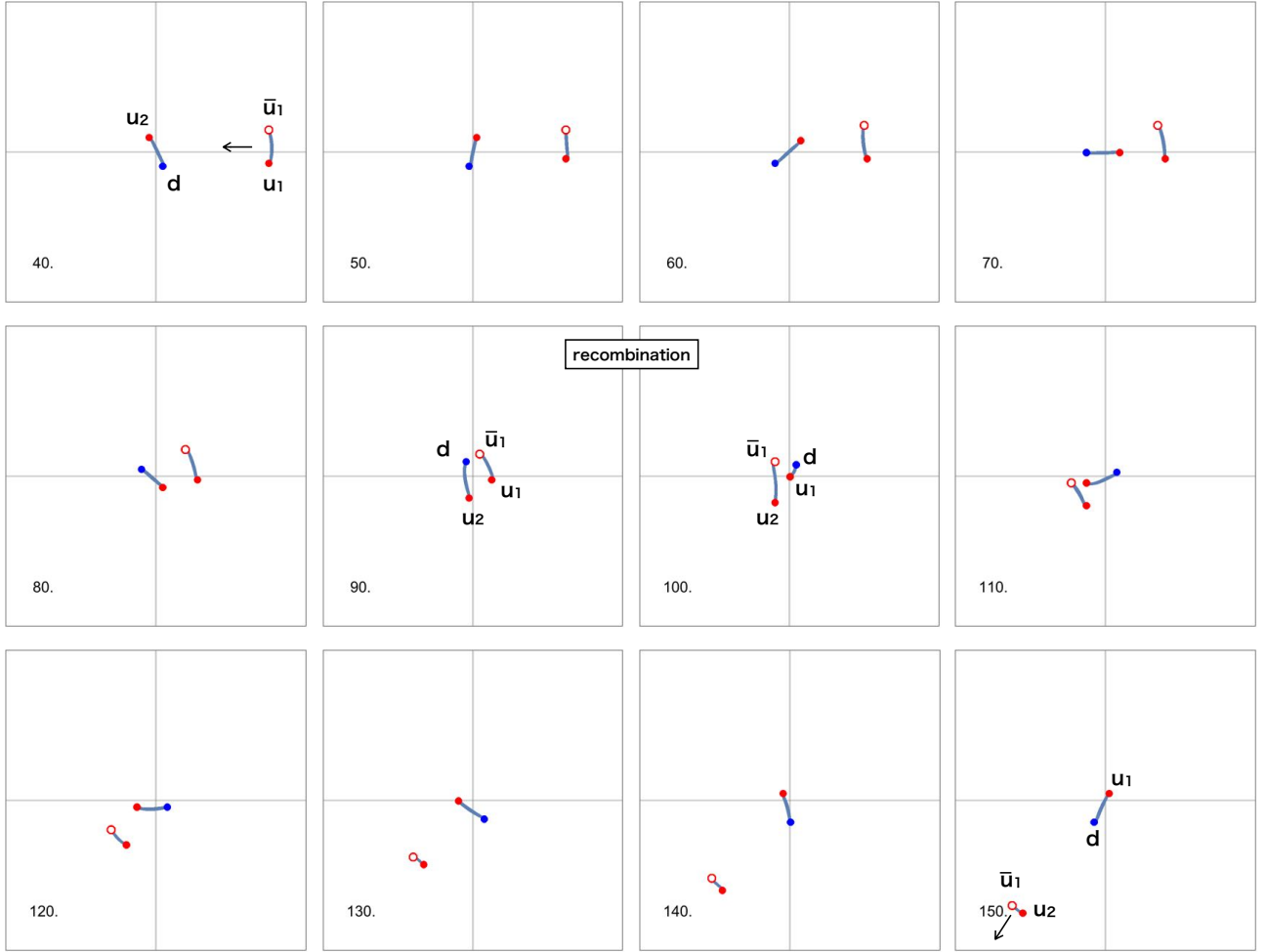


FIG. 43. The scattering of the meson $\bar{u}_1 u_1$ and the baryon $u_2 d$ with the initial configuration given in Fig. 40 (b). The collision accompanies the recombination at about $\tilde{t} = 90$. The outgoing meson is $\bar{u}_1 u_2$ and the new baryon $u_1 d$ is left near the origin. We show the snapshots from $\tilde{t} = 40$ to 150 with interval $\delta\tilde{t} = 10$, and the plot region is $\tilde{x}_{1,2} \in [-40, 40]$.

of $\bar{u}_1 u_1$ and d of $u_2 d$. Then, a new meson $\bar{u}_1 u_2$ goes away and a new baryon $u_1 d$ remains near the origin and keep rotating. We have examined lots of collisions with various initial configuration, and have found that all of them are qualitatively the same.

B. A vortical hadron jet

In high energy physics, when hadrons collide with sufficiently high energy, they fragment into quarks or gluons. However, obeying the color confinement in QCD, no color charged objects can exist alone. Therefore, these fragments create new colored particles around them to form color neutral objects, namely hadrons. A bunch of the hadrons form a narrow beam which is called a hadron jet. Since our vortices also obey the $U(1)_R$ confinement in BECs, which we have seen quite similar to QCD, we expect that a hadron jet would be observed also in BECs.

Running speed of a vortical meson is determined by length of the meson. Namely, we cannot freely change the running speed of mesons unlike relativistic particles in reality. As shorter the meson is, faster it runs. However, there is a threshold of the minimum length of the meson over which mesons are unstable to be annihilated. Therefore, we cannot give a large kinetic energy to mesons. Hence, it is not easy to set up a simulation with ultra high colliding energy in BECs. Indeed, as we have seen in the previous subsections so far, the typical scatterings do not yield any additional new hadrons. Then we change our strategy: instead of taking a shorter meson, we take a longer meson. Thus, we prepare the third initial configuration given in Fig. 40 (c) in which the baryon is the same as the one of

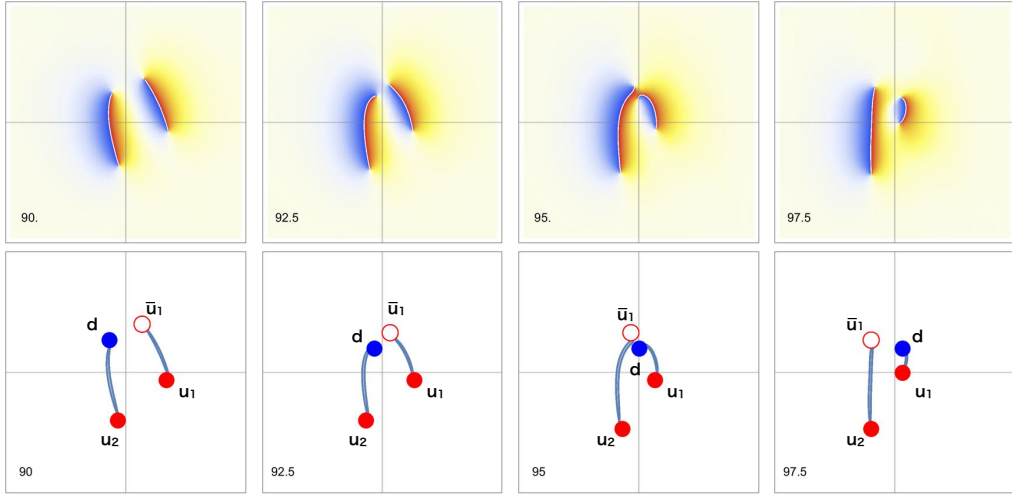


FIG. 44. Snap shots of Fig. 43 in close-up for $\tilde{x}_i \in [-15, 15]$ at $\tilde{t} = 87.5, 90, 92.5, 95$ are shown.

Fig. 40 (a) but the meson is longer. It is in Fig. 45 how the collision of a longer meson and normal baryon occurs. Since the longer meson runs slower, it takes more time to reach the target baryon at the origin. Thus, compared with Fig. 41, the baryon rotates slightly more so that the relative angle between the meson and baryon is also slightly different. However, the first reaction is not affected by such a small difference. Namely, the meson and baryon again experience the recombination accompanied by a partial annihilation of the SG and anti-SG solitons. While the corresponding vortical reaction process is the same as Eq. (24), the details of the collision are shown in Fig. 46. As before, a relatively short meson $\bar{u}_1 u_2$ and a relatively long baryon $u_1 d_1$ form during the collision. The former flies away with a smaller scattering angle. The latter baryon is very long and bended. Then it soon disintegrates into smaller hadrons. Indeed, it fragments by creating a d_2 and \bar{d}_2 in a certain point middle of the longer baryon. As a consequence, the third hadron, $\bar{d}_1 d_2$ is emitted toward the similar direction of the first meson $\bar{u}_1 u_2$. We interpret the new hadron which appears as a result of fragmentation of the confining SG soliton a vortical hadron jet, though the jet consists of only two mesons $\bar{u}_1 u_2$ and $\bar{d}_2 d_1$. The vortical reaction for it is



The third meson $\bar{d}_2 d_1$ is very short. So it crawls under waves of Ψ_i for a while and soon emerges again, see the panels with $\tilde{t} = 130$ and 140 of Fig. 45.

C. The Feynman diagrams

We have found the two new vortical reactions summarized in Eqs. (24) and (25) through the meson-baryon scatterings. They can also be described by Feynman diagrams as before. The corresponding diagrams are a meson-meson-baryon-baryon vertex and a meson-meson-baryon vertex shown in Fig. 47. The former vertex is new in a sense that any of the discrete symmetries F , T , and P cannot relate it to any of the previous diagrams shown so far. Although the latter vertex has not also been encountered yet, it can be obtained by flipping an external leg of the vertex (mbb4) of Fig. 18. However, as mentioned before, the presence (mbb4) of Fig. 18 as a real process does not immediately mean that the vertex (b) of Fig. 47 indeed occurs as a real processes. Thus, we again put our emphasis on that we include the vertex (b) of Fig. 47 into our diagram list because of the fact that we have found it in the simulation.

VI. A CONNECTION TO THE CONFINEMENT PROBLEM IN PARTICLE PHYSICS

So far, we have investigated the topological objects in non-relativistic two component BECs in 2+1 dimensions. At glance, these seem to be very far from relativistic particle physics in 3+1 dimensions. Nevertheless, the terminology (u, d, meson, baryon, and so on) and the description by Feynman diagrams borrowed from QCD are surprisingly fit BECs. Although a precise connection between QCD and BECs is not clear at all, let us try to give some hints for unveiling it along with the observations by Son and Stephanov in Ref. [8].

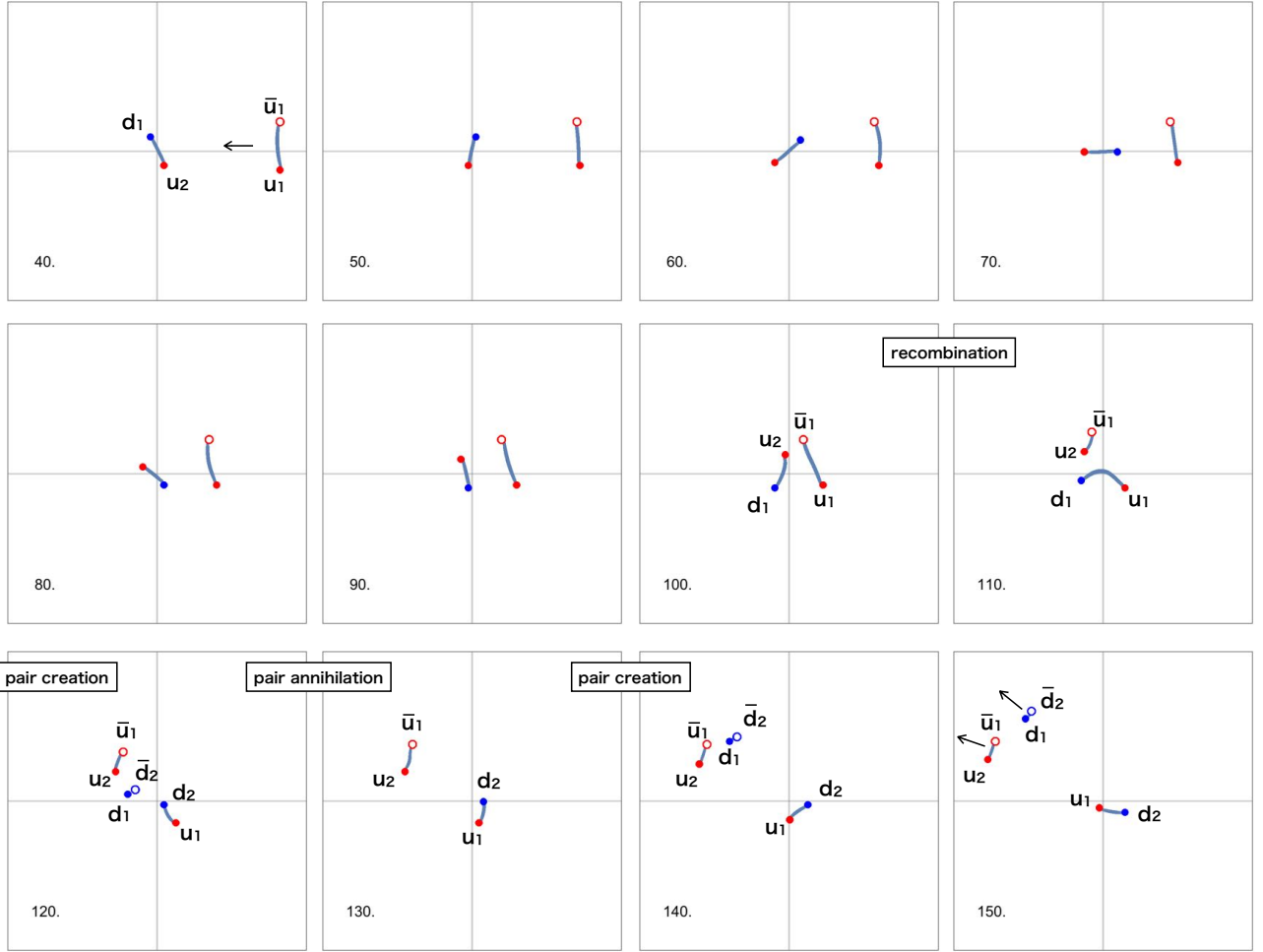


FIG. 45. The scattering of the meson $\bar{u}_1 u_1$ and the baryon $u_2 d$ with the initial configuration given in Fig. 40 (c). The collision accompanies the recombination, pair creation, and pair annihilation. A new meson $\bar{d}_2 d_1$ is emitted, which we interpret a vortical hadron jet. We show the snapshots from $\bar{t} = 40$ to 150 with interval $\delta\bar{t} = 10$, and the plot region is $\bar{x}_{1,2} \in [-40, 40]$.

The key ingredient is a duality. The vortices are particle-like topological defects in $2 + 1$ dimensions, and they are not elementary constituents of the original models. Nevertheless, it is known that a duality sometimes interchanges the defects and elementary constituents. A classic example is the duality between sine-Gordon solitons and fermions in the massive Thirring model in $1 + 1$ dimensions [39, 40]. Another simplest example more relevant to this paper is particle-vortex duality between the XY -model and the Abelian-Higgs model in $2 + 1$ dimensions [41, 42], which gives insights for understanding fractional quantum Hall effect [43]. In the particle physics context, the dualities have been expected to be one of the powerful tools for us to understand much better non-perturbative dynamics in strongly coupled systems.

On the other hand, one of the most important unsolved problems in modern high energy physics is the confinement of colors in QCD. The quarks and gluons are elementary constituents of QCD, but we cannot observe them at low energy since they are strongly confined to form hadrons. Widely accepted picture of the confinement is that chromo-electric flux from a quark is squeezed to form a flux tube. Then, interaction energy between (anti-)quarks is proportional to the distance: it is confinement. Though this picture of confinement is quite plausible, it is merely qualitative. Indeed, it is very difficult to prove analytically whether it occurs or not in real QCD. Then, instead of QCD, many studies have been done for QCD-like theories. A brilliant milestone was put by Seiberg and Witten in supersymmetric $SU(2)$ Yang-Mills theory [44, 45]. They analytically showed condensation of the magnetic monopole at low energy ground state indeed takes place.

Another, rather old back in 70s, important remark was made by Polyakov [46]. He considered a compact $U(1)$ gauge theory in $2+1$ dimensions which can be obtained as a low energy effective theory of the Georgi-Glashow model with $SU(2)$ gauge field coupled to an adjoint scalar field ϕ_a ($a = 1, 2, 3$). In the ground state, the adjoint scalar

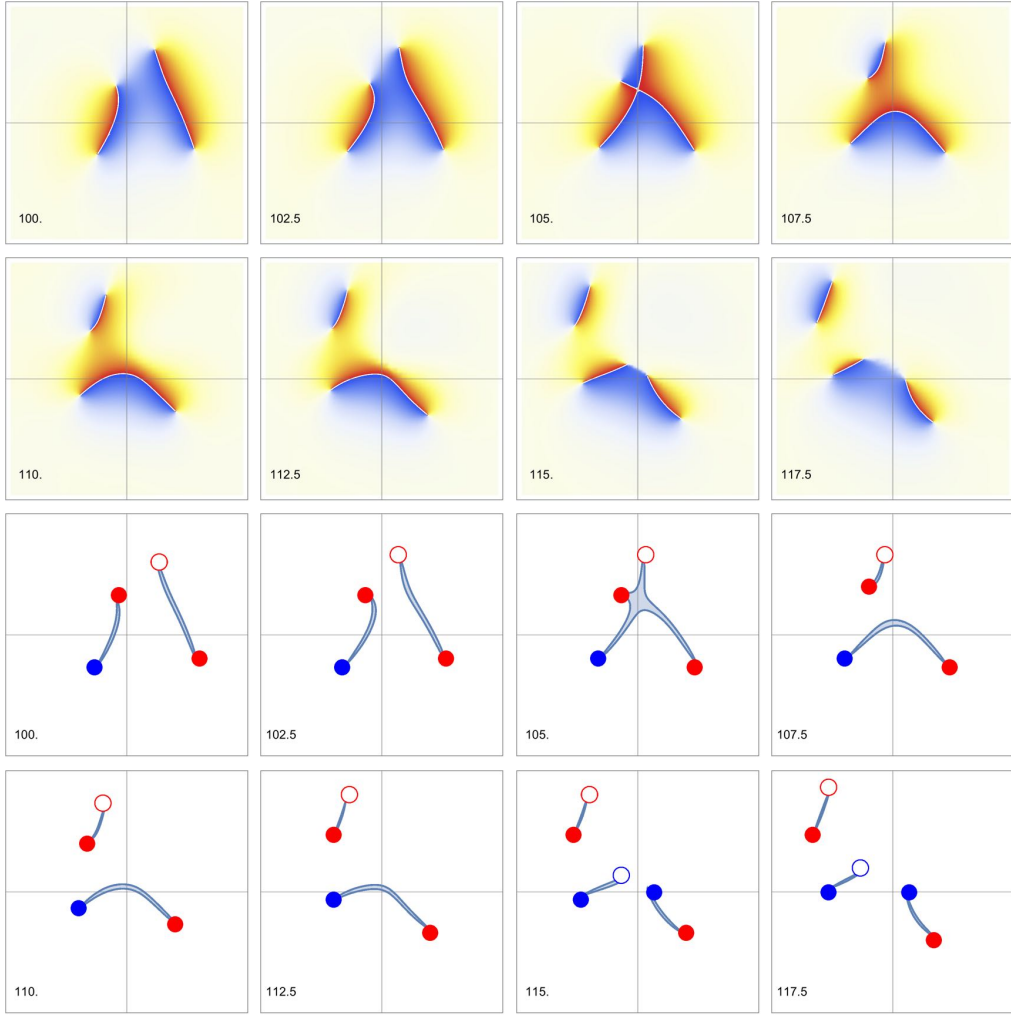


FIG. 46. Snapshots of Fig. 45 in close-up for $\tilde{x}_i \in [-15, 15]$ from $\tilde{t} = 100$ to 117.5 with interval $\delta\tilde{t} = 2.5$ are shown.

field develops a non-zero vacuum expectation value $\phi_a = (0, 0, v)$, and it breaks $SU(2)$ to its diagonal compact $U(1)$ subgroup. After integrating all the massive fields, we are left with a free massless photon of the compact $U(1)$ group at low energy. Since the photon has only one polarization in three dimensions, it can be dualized to a periodic scalar field $\vartheta \in [0, 2\pi)$, so-called dual photon which is related to the original $U(1)$ gauge field A_μ by

$$F_{\mu\nu} = \frac{e^2}{4\pi} \varepsilon_{\mu\nu\rho} \partial^\rho \vartheta, \quad F_{\mu\nu} = \partial_\mu A_\nu - \partial_\nu A_\mu, \quad (26)$$

with $\mu, \nu = 0, 1, 2$ and e is a $U(1)$ gauge coupling constant. Under the duality relation, electric charges in the original theory are interchanged by vortices in the dual theory as

$$\vartheta(z) = \sum_a q_a \text{Im} \log(z - z_a) \quad (27)$$

with $z = x + iy$. Here, z_a are positions of vortices and $q_a = \pm 1$ are their charges. The dual photon is massless in perturbation theory but it gets mass by non-perturbative instanton ('t Hooft-Polyakov type monopole) effects in the Georgi-Glashow model. In the weakly coupled region, the instantons interact with the Coulomb force and behave as a dilute plasma. Then the Debye screening effect gives a non-zero mass to the dual photon, which can be summarized in the following low energy effective theory [46–49]

$$\mathcal{L}_{\text{eff}} = \frac{e^2}{32\pi^2} \partial_\mu \vartheta \partial^\mu \vartheta + c\xi\eta^3 \cos \vartheta, \quad (28)$$

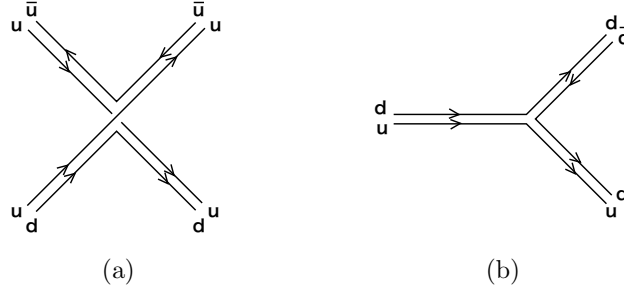


FIG. 47. (a) meson-meson-baryon-baryon vertex corresponding to the real process for Eq. (24). (b) meson-meson-baryon vertex corresponds to the real process for Eq. (25).

with c being an undetermined parameter. The dimension full parameter η is related to the mass M_W of the massive gauge bosons as $\eta^3 = M_W^{7/2}/e$. The so-called monopole fugacity ξ is exponentially small as $\xi = \exp(-\frac{2\pi M_W}{e^2}\epsilon)$ where ϵ is a function of the ratio of M_W and the Higgs mass M_ϕ , which is known to be of order one. From Eq. (28), the dual photon mass reads

$$M_\theta^2 = \frac{16\pi^2 c \eta^3 \xi}{e^2}. \quad (29)$$

The non-perturbative instanton effects is responsible for another important phenomenon, the charge confinement. Putting a probe charge in the Georgi-Glashow model corresponds to putting a vortex in the dual theory as $\vartheta = \text{Im} \log z = \theta$ ($z = r e^{i\theta}$). When we go around the vortex, ϑ passes a potential peak once at $\theta = \pi$. Namely, a semi-infinite domain wall attaches at the vortex, and it corresponds to the confining string attached to the probe charge in the original picture. This is standard understanding of the confinement in the compact QED in 2+1 dimensions.

Now we are in a position to observe a relation between the dual theory (28) and the Gross-Pitaevskii equations (1) of the 2 component BECs. The Lagrangian for Eq. (1) is given by

$$\mathcal{L}_{\text{GP}} = \sum_i \left[-\frac{i\hbar}{2} (\Psi_i \dot{\Psi}_i^* - \dot{\Psi}_i \Psi_i^*) - \frac{\hbar^2}{2m} |\nabla \Psi_i|^2 + \mu_i |\Psi_i|^2 - \frac{g_i}{2} |\Psi_i|^4 \right] - g_{12} |\Psi_1 \Psi_2|^2 - V_R, \quad (30)$$

with $V_R = -\hbar\omega (\Psi_1 \Psi_2^* + \Psi_1^* \Psi_2)$. Then we truncate this by substituting the expression of the condensates $\Psi_i = (v + r_i) e^{i\theta_i}$ into Eq. (30) and by integrating out the amplitude modes r_i [8, 16]:

$$\tilde{\mathcal{L}}_{\text{GP}} = \tilde{\mathcal{L}}_S + \tilde{\mathcal{L}}_R, \quad (31)$$

with

$$\tilde{\mathcal{L}}_S = \frac{\hbar^2}{g + g_{12}} \dot{\theta}_S^2 - \frac{\hbar^2 v^2}{m} (\nabla \theta_S)^2, \quad (32)$$

$$\tilde{\mathcal{L}}_R = \frac{\hbar^2}{g - g_{12}} \dot{\theta}_R^2 - \frac{\hbar^2 v^2}{m} (\nabla \theta_R)^2 + 2\hbar\omega v^2 \cos 2\theta_R, \quad (33)$$

where we have ignored constants and dealt with the Rabi term perturbatively. Here $\theta_S = (\theta_1 + \theta_2)/2$ is a phonon and $\theta_R = (\theta_1 - \theta_2)/2$ is known as the Leggett mode or phason. Note that the potential term in Eq. (33) is identical to V_R given in Eq. (16). Now, we would like to identify \mathcal{L}_{eff} in Eq. (28) with $\tilde{\mathcal{L}}_R$ in Eq. (33). This can be achieved by making a correspondence as

$$\vartheta \Leftrightarrow 2\theta_R, \quad (34)$$

$$\frac{e^2}{8\pi^2} \Leftrightarrow \frac{\hbar^2}{g - g_{12}}, \quad (35)$$

$$c\xi\eta^3 \Leftrightarrow 2\hbar\omega v^2, \quad (36)$$

and we have rescaled the spatial coordinate as $\tilde{x}_i = \sqrt{\frac{m}{(g - g_{12})v^2}} x_i$ in Eq. (33).

The presence of the additional massless scalar field θ_S is a crucial difference between the Polyakov's dual theory (28) and the low energy effective theory of the BECs in (31). We envisage a gauge theory whose gauge symmetry

is broken like $U(1)_S \times SU(2) \rightarrow U(1)_S \times U(1)_R$ as an electric dual of the two-component BECs. Thanks to the additional θ_S , we have two different species of the vortices, namely u- and d-vortices, and we can deal with not only the mesonic molecules but also the baryonic molecules unlike the original Polyakov's model. Furthermore, we would like to emphasize that one of the nicest virtue of the two-component BECs is accessibility to dynamical aspect of the confining phenomena as we have shown above.

Having these duality pictures in our minds, we ask ourself again what physical meaning of the Feynman diagrams is. Although we have no rigorous arguments, the classical diagrams of the u- and d-vortices would correspond to quantum Feynman diagrams of the elementary particles of the dual theory. For example, the classical 1-loop diagram in Fig. 33 seems to be mapped onto the quantum 1-loop diagram in the dual theory. If we could compute a quantum quantity from dynamics of some classical topological defects in very different theory, it is interesting. We have no further observations pushing the idea forward, so we leave it as an open question at this moment.

Finally, as a possible clue for pinning down the connection between particle physics and two-component BECs, let us briefly mention the Okubo-Zweig-Iizuka (OZI) rule [32–34] which is a phenomenological rule of QCD found in 1960s [35]. The OZI rule explains the narrow decay width of the vector meson. Kinematically, the decay $\phi(\bar{s}s) \rightarrow \pi^+(\bar{d}u) + \pi^0(\bar{d}d) + \pi^-(\bar{u}d)$ dominates the other decay process $\phi(\bar{s}s) \rightarrow K^+(\bar{s}u) + K^-(\bar{u}s)$ because the phase space of the former process is much larger than the latter. Nevertheless, the process $\phi \rightarrow 3\pi$ is highly suppressed relative to $\phi \rightarrow K^+K^-$. The OZI rule in QCD is a phenomenological postulation that diagrams with disconnected quark lines are suppressed relative to connected ones. It seems natural for us to ask whether a similar rule holds for hadronic molecules in two-component BECs or not. In order to answer this question, let us consider decay of a $\bar{u}u$ mesonic molecule, and verify if the diagrams given in Fig. 48 are observed or not. Throughout this work, we have met the decay

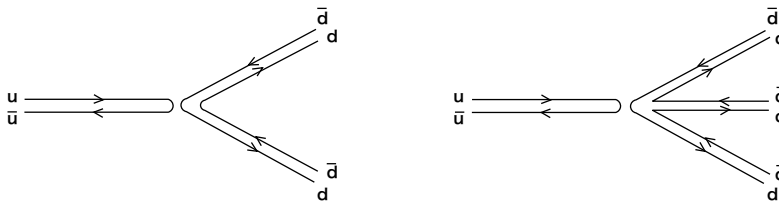


FIG. 48. Disconnected diagrams for $\bar{u}u$ decay.

diagrams of $\bar{u}u$ three times. The first and the second ones are given in Fig. 18 (mmm3) and (mbb1), respectively. The third one is the left-most diagram of Fig. 34. None of them are disconnected diagrams. Moreover, not only these three diagrams but also all the diagrams we encountered so far are connected diagrams. Thus, we have found an empirical rule that diagrams with disconnected vortex lines are highly suppressed relative to connected ones. Namely, the OZI rule seems to hold even in BECs. The OZI rule in QCD is explained as follows. Disconnected quark lines are indeed connected by internal gluon lines. High momentum transfer by the gluons makes the QCD coupling constant small, so that such channels are highly suppressed. Thus, the QCD OZI rule is a consequence of a quantum effect. On the other hand, the dynamics of vortical hadrons in BECs essentially obeyed the classical GP equations. We expect that a counterpart of the gluon is the classical wave functions Ψ_i , and the classical OZI rule in BECs corresponds to the quantum OZI rule in QCD via a duality. As we repeated, we do not have a precise connection between QCD and BECs. This is an open question.

VII. SUMMARY AND DISCUSSION

In this work, we have investigated dynamics of the vortex molecules in two-component BECs by numerically solving the Gross-Pitaevskii equations (1). This paper is on the line of the previous works [8, 14, 16] focusing on the confinement property of fractional vortices by the SG solitons. While the dynamical property of an individual molecule, such as precession and disintegration, were figured out in Refs. [14, 16], here we have studied the scattering and collision of molecules. Our numerical studies are twofolds: the meson-meson scattering and the meson-baryon scattering.²

² For both the simulations, the non-relativistic nature of the GP equations is crucial since it ensures that the molecule size is kept to be finite and constant even though the constituent vortices are pulled by the SG soliton. In relativistic models, this cannot happen because the molecules soon shrink. Especially, it is very difficult to prepare mesonic molecules which soon decay into radiations. Cost we have to pay is that both the precession speed of a baryonic molecule and the translation speed of a mesonic molecule are determined by the molecule size [16], but we can, nevertheless, make use of such dynamical properties (the precession of baryons and the translation of mesons) for planning scattering experiments of the mesons and baryons. Indeed, our numerical simulations provide quite rich and interesting results as we have described above in details.

In Sec. III, we have dealt with the meson-meson scattering of the same spices ($\bar{u}u$ - $\bar{u}u$). Firstly, we have demonstrated three simulations of the head-on collisions (zero impact parameter) by varying the incident angles, which are summarized in Fig. 14. We have found that the mesons collide involving the vortical reaction given in Eq. (20). Namely, the constituent vortices swap the partners. We also showed that the recombination can be understood as a collision of the SG and anti-SG solitons, and the swapping is nothing but the pair annihilation and creation of the confining SG solitons as can be seen in Fig. 7. Of course, the details of the final states sensitively depend on the initial incident angles. The simulation with the initial relative angle π happens to show the right angle scattering of the two mesons, which is very common among relativistic topological solitons. On the other hand, the scattering with smaller angle $\pi/2$ exhibits more complicated out-going state involving the pair creation of a new meson and a subsequent pair annihilation of the original meson. In principle, there are thousands of different scatterings depending on the model parameters, initial configurations, and so on. Clearly, solving numerically the GP equations for each time is not a good strategy. To avoid such infinitely high cost surveys and to get efficient outlook, we developed a useful description by using the Feynman diagrams. A fractional vortex corresponds to a line with an arrow toward the time direction whereas an anti-fractional vortex is expressed by a line with an arrow opposite to the time direction. The elementary vertices found through the meson-meson scatterings with an aid of time reversal and the parity transformations are summarized in Fig. 18. These are building blocks of the real scattering processes. We also have studied the meson-meson scatterings with non-zero impact parameters. It is found that the scattering angles depend on the impact parameter: the smaller impact parameter is, the larger the scattering angle is. As increasing the impact parameter, the scattering angle reduces and it crosses zero and becomes negative. Then, it asymptotically becomes zero as the impact parameter is taken to be infinity.

In Sec. IV, we have turned to studying the meson-meson scattering of the different spices ($\bar{u}u$ - $\bar{d}d$). We have repeated the numerical simulations similar to those in Sec. III. The head-on collision with the 0 relative angle seems to be boring at glance: the two mesons just pass through, see Fig. 24. However, we have found that the scattering of the two SG solitons occurs. They bounce off, and the molecules interchange the SG solitons before and after the collision. The head-on collisions with the smaller relative angles are more interesting. We have found that the incoming u and d mesons are converted to the intermediate baryon and anti-baryon pair during the collision. The intermediate baryons rotate, and then they are reformed back into the mesons at the second recombination. Forming the intermediate baryonic state results in the shift of the outgoing line from the ingoing one, see Fig. 32. As before, we have described the numerical simulations by using the Feynman diagrams, and divided them into the elementary vertices. The newly found vertices are shown in Figs. 33. In addition, we also have put the new vertices in Figs. 34 and 35, corresponding to the disintegrations of the meson and baryon found in Refs. [14, 16]. We also have studied the scatterings with non-zero impact parameters but the results are not so dramatic as those for the mesons of the same spices.

In Sec. V, we have studied the meson-baryon scatterings ($\bar{u}u$ and ud). We have injected the meson toward the baryon staying at the origin. A variety of the scatterings arises from the difference of the relative angles of the two molecules at the collisions. We have examined two initial configurations (the molecules are initially parallel and anti-parallel) given in the left-most and the middle panels of Fig. 40. We have found that there are no qualitatively large differences between the two cases. In the both cases, the meson and baryon swap their constituent u vortices, and the new meson goes out while the new baryon stays at slightly shifted point from the original baryon point. Much more interesting thing happens when we scatter a longer meson to the baryon. The typical initial configuration is given in the right-most panel of Fig. 40, and the scattering goes as shown in Fig. 45. The recombination takes place also in this case, so that a longer and kink bend baryon is formed at first stage. However, such a long and bent molecule is unstable and soon disintegrates into a set of shorter meson and baryon. As a result, the final state includes larger number of molecules than the prepared one. This somehow resembles what happens in real Hadron collider experiments. When we collide two hadrons in a Hadron collider with sufficiently large energy, thousands of hadrons come out as a hadron jet. Although our final state consists of only a few hadrons, we exaggeratedly call it a vortical hadron jet in the VHC (vortical hadron collider) experiment. It is surprising to us that the simple classical system (1) include such rich phenomena somehow common to QCD which needs highly quantum regimes.

In Sec. VI, we have made supplementary comments to make a connection between QCD and BECs clearer. We have compared the Polyakov's dual photon model in $2 + 1$ dimensions to the low energy effective theory based on the two-component BECs. We have seen the latter is an extension of the former, and so we expect the confinement of the u - and d -vortices studied here would shed some lights to the confinement of the elementary particles. A good advantage using the BECs is that we can easily access to dynamical aspects of the confinement which is in general difficult. As a related topic, we also have pointed out that the similar rule to the OZI rule in QCD seems to hold in the BECs.

To close this paper, let us list what we have not done in this work. All numerical analysis in this paper have been done under the condition (2). Therefore, the u - and d -vortices have the same masses. The dynamics of the hadronic molecules for generic cases will be surely more complicated, but they might be more similar to QCD since the quarks have different masses in nature. Furthermore, we considered the model with two condensates. It is the reason why

we have two different species, the u- and d-vortices. If we include three or more condensates, we can consider hadrons consisting of more than two constituent vortices [23, 24]. It would be especially interesting to study molecules such as a proton like molecule uud and a neutron like molecule udd to simulate situations closer to QCD. It might be also interesting to take into account the vortical hadrons at finite temperature and/or density. In QCD, there exist several phases such as quark gluon plasma and color superconducting phase. Exploring the phase diagram of the vortex matter in BEC would shed some light on the phase diagram of real QCD, see Ref. [50] for vortices in color superconductors in QCD.

Acknowledgments

This work was supported by the Ministry of Education, Culture, Sports, Science (MEXT)-Supported Program for the Strategic Research Foundation at Private Universities “Topological Science” (Grant No. S1511006) and JSPS KAKENHI Grant Numbers 16H03984. The work of M. E. is also supported in part by JSPS Grant-in-Aid for Scientific Research KAKENHI Grant No. JP19K03839, and by MEXT KAKENHI Grant-in-Aid for Scientific Research on Innovative Areas “Discrete Geometric Analysis for Materials Design” No. JP17H06462 from the MEXT of Japan. The work of M. N. is also supported in part by JSPS KAKENHI Grant Number 18H01217 by a Grant-in-Aid for Scientific Research on Innovative Areas “Topological Materials Science” (KAKENHI Grant No. 15H05855) from MEXT of Japan.

-
- [1] F. Dalfovo, S. Giorgini, L. P. Pitaevskii and S. Stringari, *Rev. Mod. Phys.* **71**, 463 (1999).
 - [2] L. Pitaevskii and S. Stringari “Bose-Einstein Condensation and Superfluidity,” (Oxford University Press, 2003),
 - [3] C. J. Pethick, and H. Smith, “Bose-Einstein Condensation in Dilute Gases,” (Cambridge University Press, 2008).
 - [4] A. L. Fetter, *Rev. Mod. Phys.* **81**, 647 (2009).
 - [5] D. V. Freilich, D. M. Bianchi, A. M. Kaufman, T. K. Langin, and D. S. Hall, *Science* **329**, 1182 (2010); S. Middelkamp, P. J. Torres, P. G. Kevrekidis, D. J. Frantzeskakis, R. Carretero-Gonzalez, P. Schmelcher, D. V. Freilich, D. S. Hall, *Phys. Rev. A* **84** 011605(R) (2011); R. Navarro, R. Carretero-Gonzalez, P. J. Torres, P. G. Kevrekidis, D. J. Frantzeskakis, M. W. Ray, E. Altuntas, and D. S. Hall, *Phys. Rev. Lett.* **110**, 225301 (2013).
 - [6] D. S. Hall, M. R. Matthews, J. R. Ensher, C. E. Wieman, and E. A. Cornell, *Phys. Rev. Lett.* **81**, 1539 (1998).
 - [7] M. R. Matthews, D. S. Hall, D. S. Jin, J. R. Ensher, C. E. Wieman, E. A. Cornell, F. Dalfovo, C. Minniti, and S. Stringari, *Phys. Rev. Lett.* **81**, 243 (1998); M. R. Matthews, B. P. Anderson, P. C. Haljan, D. S. Hall, M. J. Holland, J. E. Williams, C. E. Wieman, and E. A. Cornell, *Phys. Rev. Lett.* **83**, 3358 (1999); B. P. Anderson, P. C. Haljan, C. E. Wieman, and E. A. Cornell, *Phys. Rev. Lett.* **85**, 2857 (2000).
 - [8] D. T. Son and M. A. Stephanov, *Phys. Rev. A* **65**, 063621 (2002)
 - [9] J. J. Garcia-Ripoll, V. M. Perez-Garcia, and F. Sols, *Phys. Rev. A* **66**, 021602 (2002).
 - [10] K. Kasamatsu, M. Tsubota and M. Ueda, *Phys. Rev. Lett.* **93**, no. 25, 250406 (2004)
 - [11] K. Kasamatsu, M. Tsubota and M. Ueda, *Int. J. Mod. Phys. B* **19**, 1835 (2005).
 - [12] M. Cipriani and M. Nitta, *Phys. Rev. Lett.* **111**, 170401 (2013).
 - [13] M. Nitta, M. Eto and M. Cipriani, *J. Low. Temp. Phys.* **175**, 177 (2013)
 - [14] M. Tylutki, L. P. Pitaevskii, A. Recati and S. Stringari, *Phys. Rev. A* **93**, no. 4, 043623 (2016).
 - [15] L. Calderaro, A. L. Fetter, P. Massignan, P. Wittek, *Phys. Rev. A* **95**, no. 1, 023605 (2017).
 - [16] M. Eto and M. Nitta, *Phys. Rev. A* **97**, no. 2, 023613 (2018).
 - [17] M. Kobayashi, M. Eto and M. Nitta, *Phys. Rev. Lett.* **123**, no. 7, 075303 (2019).
 - [18] A. Usui, H. Takeuchi, *Phys. Rev. A* **91**, 063635 (2015).
 - [19] C. Qu, L. P. Pitaevskii, S. Stringari, *Phys. Rev. Lett.* **116**, 160402 (2016).
 - [20] C. Qu, M. Tylutki, L. P. Pitaevskii, S. Stringari, *Phys. Rev. A* **95**, 033614 (2017).
 - [21] K. Ihara and K. Kasamatsu, *Phys. Rev. A* **100**, 013630 (2019).
 - [22] P. Kuopanportti and J. A. M. Huhtamäki and M. Möttönen, *Phys. Rev. A* **83**, 011603(R) (2011).
 - [23] M. Eto and M. Nitta, *Phys. Rev. A* **85**, 053645 (2012).
 - [24] M. Eto and M. Nitta, *Europhys. Lett.* **103**, 60006 (2013).
 - [25] M. Cipriani and M. Nitta, *Phys. Rev. A* **88**, 013634 (2013).
 - [26] D. S. Dantas, A. R. P. Lima, A. Chaves, C. A. S. Almeida, G. A. Farias and M. V. Milošević, *Phys. Rev. A* **91**, 023630 (2015) doi:10.1103/PhysRevA.91.023630 [arXiv:1504.03203 [cond-mat.quant-gas]].
 - [27] N. V. Orlova, P. Kuopanportti and M. V. Milošević, *Phys. Rev. A* **94**, 023617 (2016).
 - [28] S. H. Shinn and U. R. Fischer, *Phys. Rev. A* **98**, no. 5, 053602 (2018).
 - [29] Y. Nambu, *Phys. Rev. D* **10**, 4262 (1974).
 - [30] G. 't Hooft, in Proc. of the E.P.S. Int. Conf. on High Energy Physics, Palermo, 23-28 June, 1975 ed. A. Zichichi (Editrice Compositori, Bologna, 1976);
 - [31] S. Mandelstam, *Phys. Rept.* **23**, 245 (1976).
 - [32] S. Okubo, *Phys. Lett.* **5**, 165 (1963).

- [33] G. Zweig, CERN-TH-401.
- [34] J. Iizuka, Prog. Theor. Phys. Suppl. **37**, 21 (1966).
- [35] H. Fritzsch, “Murray Gell-Mann and the Physics of Quarks,” Springer, doi:10.1007/978-3-319-92195-2
- [36] M. Eto, K. Kasamatsu, M. Nitta, H. Takeuchi and M. Tsubota, Phys. Rev. A **83**, 063603 (2011).
- [37] M. Kobayashi and M. Nitta, J. Low. Temp. Phys. **175**, 208 (2014) doi:10.1007/s10909-013-0977-4 [arXiv:1307.1345 [cond-mat.quant-gas]].
- [38] K. Kasamatsu, M. Eto and M. Nitta, Phys. Rev. A **93**, no. 1, 013615 (2016).
- [39] S. R. Coleman, Phys. Rev. D **11**, 2088 (1975).
- [40] S. Mandelstam, Phys. Rev. D **11**, 3026 (1975).
- [41] M. E. Peskin, Annals Phys. **113**, 122 (1978).
- [42] C. Dasgupta and B. I. Halperin, Phys. Rev. Lett. **47**, 1556 (1981).
- [43] D. H. Lee and M. P. A. Fisher, Phys. Rev. Lett. **63**, 903 (1989).
- [44] N. Seiberg and E. Witten, Nucl. Phys. B **426**, 19 (1994) Erratum: [Nucl. Phys. B **430**, 485 (1994)].
- [45] N. Seiberg and E. Witten, Nucl. Phys. B **431**, 484 (1994).
- [46] A. M. Polyakov, Nucl. Phys. B **120**, 429 (1977).
- [47] I. I. Kogan and A. Kovner, In *Shifman, N. (ed.): At the frontier of particle physics. Vol. 4* 2335-2407 doi:10.1142/9789812777270_0003 [hep-th/0205026].
- [48] D. Antonov and M. C. Diamantini, In *Shifman, M. (ed.) et al.: From fields to strings, vol. 1* 188-265 doi:10.1142/9789812775344_0011 [hep-th/0406272].
- [49] M. Shifman and M. Unsal, Phys. Rev. D **78**, 065004 (2008).
- [50] M. Eto, Y. Hirono, M. Nitta and S. Yasui, PTEP **2014**, no. 1, 012D01 (2014) doi:10.1093/ptep/ptt095 [arXiv:1308.1535 [hep-ph]].